GEM-TN-93-301
GEM/CSC 2-93

Interpolating Cathode Strip Chambers of the GEM Muon System

Prototype Development and Performance
Draft

V.A. Polychronakos
for the CSC Group

February 4, 1993

BROOKHAVEN NATIONAL LABORATORY

February 4, 1993 GEM/CSC 2-93

DRAFT
February 4, 1993

The Interpolating Cathode Strip Chambers of the GEM Muon System

Prototype Development and Performance

V.A. Polychronakos
for the CSC Group

1 Introduction

A series of interpolating Cathode Strip Chamber(CSC) prototypes have been constructed in our effort to develop the CSC technology for application to the Muon System for GEM. These prototypes include a "full scale" (1.8x1.2m^2) four-layer module (at BNL), a large (1.5x1m^2) module at Dubna, three ≈0.5x0.5m^2, four-gap chambers, one with radial strips (Boston U.), one with parallel strips (BNL), and a similar one at PNPI but using a construction technique more suitable for mass production. A number of small, specialized chambers to study a variety of parameters relevant to the CSC operation were also built at BNL, PNPI, and Boston University. In addition a 1x0.5m^2 prototype using Iarocci-type tubes with a cathode strip readout has been constructed by the Houston University group.

The emphasis, throughout this R&D program, has been on developing and understanding all aspects of this technology. An appropriate, nonflammable gas has been identified meeting all requirements of the full detector. Single layer spatial resolution better than the 75μm required by the baseline design has been achieved in both small and large prototypes. Efficient bunch crossing timing was demonstrated by identifying the earliest signal arrival from 4 or 6 layers using a simple OR circuit. The tagging efficiency ranges from 92% (with 6 layers and simple time- over-threshold discriminators) to 100% (four layers with constant fraction discriminators). Chamber efficiency better than 99% with either anode or cathode signals has been achieved.

The importance of a relatively simple, robust, low cost electronic readout system in achieving 1% measurements with a detector with $\approx 10^6$ channels was recognized. An aggressive, two-prong approach has been followed:

- A compact, low cost, highly multiplexed readout system for the prototypes was developed utilizing existing monolithic amplifiers augmented by custom hybrid preamplifiers. Most of the prototypes are tested fully instrumented. The "small" BNL four layer module, for example, has 288 cathode and 32 anode channels. The large four layer module will have a total of 704 cathode channels (only two layers have been tested todate, the other two are nearing completion and are expected to be delivered at the SSC at the end of February). It should be noted that the largest Barrel module will have no more than about 1000 channels.

- In parallel, an effort to develop a custom monolithic front end suitable for the GEM muon detector subsystem was launched. Prototype circuits featuring a low noise preamplifier, shaper, and sample and hold have already been fabricated and tested.

Alignment is another crucial factor in achieving the baseline performance. A novel alignment system is being developed utilizing collimated high energy (36 keV) X-rays which are directly detected by the CSCs providing relative alignment of all layers of a superlayer and, possibly, between superlayers. Promising results were recently achieved by the PNPI group.

2 Prototype Development

2.1 Mechanical construction

Almost all CSC prototypes are built as two-gap modules. The two gaps are formed by three flat, rigid panels made of a 23 mm thick sheet of nomex honeycomb and two 1.25 mm thick copper-clad FR4 laminates. The 0.5 oz/ft^2 copper (17 μm thick) forms the cathodes of the two proportional chambers. The panel frames were made of machined zelux (fiberglass reinforced lexan). They provide the 2.5 mm step for the anode plane of gold-plated tungsten wires 30 μm in diameter with a 2.5mm pitch. The frames of the outer panels have a milled cavity with enough room for the epoxy beads for the wire attachment as well as the anode blocking capacitors. A rubber gasket just outside this cavity provides the gas seal for the assembly. In this manner no components under high voltage are outside the seal thus minimizing the risk of high voltage breakdowns. This technique has been successfully used in several chamber designs by the MPS group at BNL. A mechanical drawing of one of these panels is shown in Figure 1 with a more detailed view of the frame cross sections in Figure 2. The sensitive area of this prototype is 45x37 cm^2. A drawing of the two-gap assembly (for the large trapezoidal prototype) is shown in Figure 3.

The position sensing cathode strips are lithographically etched on either side of the central panel. These cathodes are precisely positioned with respect to each other with the aid of locating pins. The strips are oriented at 90° with respect to the anode wires providing the precision position measurement in a direction along the wires.

On one of the continuous cathodes four windows of approximately 4x3 cm^2 were cut out. Four collimators made of 0.025″ half hard brass shim stock were placed in these windows. Each collimator has 25 slits 100 μm wide, 1.5 cm long cut every 1 mm. A drawing of one of these is shown in Figure 4. A thin layer of mylar glued on the back side of the collimators guarantees the integrity of the gas volume. Corresponding windows were opened on the outside skin of this panel to allow penetration of the soft X-rays from an ^{55}Fe source.

2.2 Position sensing cathode geometry

Seen as gaseous detectors the CSCs are Multiwire Proportional Chambers with a symmetric cell in which the anode-cathode spacing, h, is equal to the wire pitch, s, which equals 2.5 mm. The readout pitch, w_r, is 5 mm.[1] Thus the ratio of the readout pitch to anode-cathode spacing is $w_r/h = 2$. Such a high ratio results in significant (>50%) position encoding differential non-linearity since the FWHM of the cathode induced charge is about 1.5h. It has been shown [1],[2],[3] that the condition for negligible (≈1%) differential non-linearity is $w_r/h \leq 0.8$. This condition would dictate a readout pitch of 2 mm resulting in an unacceptably large number of channels. E. Mathieson and G. C. Smith have shown that linearity of response can be restored to near optimum with the use of intermediate strips between readout nodes which provide increased charge sampling frequency and are capacitively coupled to the adjacent readout strips.[4] We used an arrangement with two intermediate strips which is shown in Figure 5 along with the equivalent electrical circuit. For this capacitive interpolation to work the interstrip capacitance, C_1, must be much larger than that of a strip to ground, C_0. ($C_1/C_0 \geq 10$). For the present design of the CSCs, $C_1/C_0 \approx 10$–12. Further optimization results in intermediate strips of a slightly larger width than the readout strips.[5] In Figure 6 the expected differential nonlinearity is shown as a function of the readout strip width (expressed as fraction of the width this strip would have for the case of equal strip widths) and for several ratios C_1/C_0. For the prototypes the gap between strips is 0.250 mm, the readout strip width is 1.1 mm and that of the two intermediate strips 1.57 mm. It is necessary to provide a high resistance path to ground to avoid charge buildup on the intermediate strips. A thin strip of resistive epoxy (conductivity 6 MOhm per square) was silk screened on the tips of the strips at the end of the cathode opposite to the amplifiers.

3 Electronic Readout

The fine granularity of the CSC detectors results in a large number of channels (of order 10^6 for the entire system). In addition, the 1% charge measurement required in order to achieve the single layer resolution of the baseline design makes the readout system the most critical component of a CSC based muon detector system. Development of a credible readout system has always been a high priority item within the CSC group We adopted an aggressive, two pronged approach with the following goals:

- To fully equip the prototype modules with an electronic readout chain that closely resembles the architecture to be eventually used for the detector.
- To immediately start the development of a custom monolithic front end integrated circuit which will be the basis for a highly multiplexed, compact readout system that could be tested at the earliest possible time.

The following subsections describe the progress on these two fronts.

[1]This is true for 3/4 of the area of the detectors. For the remaining the pitch was increased to 7 mm.

3.1 Cathode Strip Readout

The spatial resolution of the CSCs depends linearly on the signal to noise ratio. For a given gas gain the lowest possible electronic noise results in optimum resolution. Note that one can not arbitrarily increase the gas amplification in order to compensate for poor noise performance. It has been shown[6] that for most gases the resolution degrades rapidly for anode charge larger than $\approx$1 pC due, primarily, to photon mediated avalanche fluctuations.

We have designed a readout system which features a high performance, low noise, hybrid, charge integrating preamplifier followed by a 16-channel monolithic shaping amplifier with multiplexed output. This CMOS integrated circuit (AMPLEX) [7]was designed at CERN for silicon detector applications and hence the need for a different front end.A block diagram of the cathode readout is shown in Figure 7 and a schematic diagram of the preamplifier is given in Figure 8. It has a JFET front end (Interfet NJ132L) optimized for an input electrode capacitance range of 50–150 pf corresponding to cathode strip lengths of 1–3 m. The feedback capacitor is 5 pf and the feedback resistor 50 MOhm so that it contributes negligible parallel noise even for long shaping times. A single transistor inverter matches the polarities of the two amplifiers and provides an additional gain of 3–4. This compensates for a gain loss of about the same factor when the AMPLEX amplifier is coupled to the hybrid with a 1.35 pf capacitor. This coupling mode allows the AMPLEX amplifier to operate with an effective input capacitive load of only 1.35 pf, close to its optimum. Although the monolithic AMPLEX still dominates the amplifier noise ($\approx$1200 equivalent rms electrons) the noise slope as a function of input capacitance is now determined by the hybrid and is only 7 electrons/pf for the shaping time of 550 ns. Had the AMPLEX amplifier been the front end this slope would have been 40–80 electrons/pf (depending on the amplifier bias current).

The multiplexed outputs from all amplex chips are buffered and sent to an on-board unity gain summing node. Up to 512 multiplexed channels are output on a single cable. Two such groups for a total of 1024 channels are read by a single CAMAC module.[8] This module digitizes the analog signals with an 8-bit flash ADC, subtracts prestored pedestals for all channels, suppresses empty channels, and builds a list of the addresses of the strips with a signal above an individually adjustable threshold and its corresponding amplitude. It results in a compact, low cost readout system with a small number of cables (less than ten for our 800 channel prototype). This immensely facilitates the task of effectively shielding the modules against electromagnetic interference as well as controlling ground loops, the bane of precision measurements in large systems.

3.2 Calibration of the Cathode Readout System.

Knowledge of the relative electronic gains in neighboring channels at the $\leq$1% level is necessary to achieve the design spatial resolution of 75μm. Precision calibration capacitors were built into the multilayer readout printed circuit board. The value of these capacitors was 0.65 pf and their uniformity was measured with a precision bridge to be better than 0.5%. Every fourth capacitor was connected to the same calibration line which was terminated into 50 Ohms. The resulting four calibration lines were fed by the same precision pulser, one at a time via a computer controlled wide-band router. The amplitude of the precision pulser as

well as its trigger were also computer controlled. At regular intervals calibration data were taken by stepping the pulser amplitude through 30 values spanning the whole dynamic range in use. A few hundred events were accumulated for every pulser value and the mean values and rms deviations calculated for all channels. A third order polynomial was then fitted to these values. This was necessary because in order to gain as much dynamic range as possible we used the AMPLEX chip in a region well beyond its linear range. Figure 9a shows one such calibration curve and corresponds to the response of the AMPLEX. The fit coefficients were then recorded and used to correct the amplitudes during data analysis. In order to check this calibration procedure a known pulse was injected in all channels. The values read back were corrected and are plotted in Figure 9b. The distribution of their variations from the nominal is plotted in Figure 9c and has a sigma of 0.55%.

3.3 Anode Readout

The anode readout is far less demanding in spite of the fact that fast shaping is required (30 ns) in order to provide trigger information and bunch crossing tagging. No amplitude information is necessary. The anode wires are connected in groups of 20 providing 5 cm wide hodoscope elements. We used the bipolar, grounded-base amplifier shown in Figure 10 (BNL Instrumentation Division, IO-354-2) and a 30 ns shaping amplifier shown in Figure 11 (BNL Instrumentation Division, IO-638-01). These are implemented in thin film hybrid technology and are mounted on a printed circuit board on the detector. They are followed by on-board discriminators which provide a fast OR for self-triggering. Thus the module is self-sufficient not requiring any additional detectors in order to be tested with sources, cosmic rays, or particle beams. The discriminator outputs are available for input into TDCs to obtain additional information during the tests although they will not be used in the final detector.

3.4 Development of a Monolithic Front End

A custom monolithic front end has been designed and prototypes have already been fabricated and are currently undergoing tests at BNL. The prototype chips contain 8 channels each of which consists of a charge-sensitive, folded cascode preamplifier, a fourth order semi-gaussian shaper with 750 nsec integration time, and a track and hold circuit. The 2μm Orbit process was used . Details of the design of this chip can be found elsewhere[9]. Figure 11a shows the noise of the preamplifier as a function of the input capacitance (top), and the linearity of response (bottom). Notice that the noise slope is just about 7 equivalent rms electrons/pf, a performance that rivals the best discrete component hybrid preamplifiers.

Work on the anode readout is also in progress although it is not as advanced as the one described above. A design has already been completed, however, and is in the process of the circuit layout. The bibolar technology (Tektronix quick chip) has been chosen as more efficient for the short integration time ($\approx$30nsec) needed for the anode readout. Simulations of the circuit show that 7 nsec rise time can be achieved even for electrodes with input capacitance as high as 300pf (equivalent to the capacitance of approximately 40 wires).

4 Prototype Performance

4.1 Gas Amplification and Gain Uniformity

The chamber gas used for all the data discussed in this report was a mixture of 90%Ar + 10%CH_4. This gas is not only readily available in premixed form but also essential for meaningful resolution measurements using the 5.9 keV X-rays from an ^{55}Fe source as will be discussed later on. These soft X-rays can not penetrate the honeycomb panels. For studies of the gain uniformity we used the 60 keV X-rays from an ^{241}Am source. Such energetic X-rays, however, produce ionization over a large area of the detector making quantitative measurements difficult. An unexpected benefit of using copper cathodes is a 8 keV Cu fluorescence line quite distinctly visible in our chambers. Using this peak in the Am spectrum we were able to measure the gas gain in the entire chamber area. Figure 12a shows the percent gain variation from a mean gain at various positions of one of the planes. In Figure 12b a histogram of these deviations is shown. All gains are contained within $\pm 20\%$ indicating that the cathode flatness (peak to peak variation) was not more that $\approx 75\mu m$.

The absolute gas gain was measured using the ^{55}Fe source illuminating the chamber through one of the four collimators. Both the cathode strips and the anode wires were used in independent measurements. A QVT was attached to the output of the shaper of one of the wire channels since no analog measurement is built-in. For the cathodes the strip with the largest pulse height was identified and then the amplitudes of its four nearest neighbors were added to that to obtain the total charge. Consistent results were obtained with both methods. In both cases the fraction of the charge collected was taken into account in order to estimate the true gain. Figure 13 shows the gas amplification as a function of the anode voltage. Most of the data discussed here were obtained with a high voltage of 1575 V corresponding to a gas gain of 2×10^4.

4.2 Single Layer Spatial Resolution

To determine the spatial resolution of the prototypes the ^{55}Fe source was placed at a distance of 25 cm from the window of one of the brass collimators to minimize the angular divergence of the photons entering the $100\mu m$ wide slits. An additional collimator was placed directly on the honeycomb panel restricting the overall illumination to about 1cm. The signal from the wire plane was used to trigger the data acquisition system. The precision coordinate of the photon absorption position was reconstructed using the following simple algorithm. The strip with the highest amplitude was identified and the induced charge centroid was calculated using this strip as well as its four nearest neighbors. The calibration constants were used to correct the amplitudes for gain variations as described earlier. No cuts were applied in energy or otherwise. A histogram of the reconstructed coordinate is shown in Figure 14a. The image of the collimator slits can be seen. Three of the histograms magnified are shown in Figure 14b. The standard deviations of the observed peaks are typically 50–$60\mu m$. They represent convolutions of a square distribution $100\mu m$ wide with a resolution function (presumed to be Gaussian). The following simple Monte Carlo method was used to unfold this resolution. A uniformly random distribution $100\mu m$ was generated. Each point was smeared by a gaussian distribution with a given σ. This was repeated with sigmas

ranging from 10 to 100 microns. In Figure 15 is shown the width of the composite distribution as a function of the width of the convolving gaussian. One notes that for infinitely good resolution the observed width would be $\approx 30\mu m(100/\sqrt{12})$. The resolution dominates the width for $\sigma > \approx 60\ \mu m$. The observed widths of 50–60μm correspond to single layer spatial resolutions of 40–50 μm. It should be noted that the photoelectron range limits the resolution to about 40 microns. Fischer, Radeka, and Smith[6] in an extensive study using a chamber designed so that all other limitation to the resolution were small compared to the contribution of the photoelectron range, measured a resolution of about 40 microns using the same gas.

The total capacitive load on each readout node was measured to be 26 pf. Capacitors of 100 pf were added to all nodes to simulate 2.5 m long strips. The resolution (without increasing the gas gain) degraded to about 75μm.

4.3 Linearity of Response

The reconstructed versus true [2] positions of the slits are plotted in Figure 16a. The solid line is a least squares fit of the data to a straight line. It can be seen that the capacitive interpolation with the aid of the two floating strips restores the linearity of response in spite of the fact that the ratio of the readout pitch to the anode-cathode distance is 2.0. There is, however, a residual nonlinearity as can be seen from Figure 15b where the variation of the reconstructed positions of the slits from the straight line fit is plotted. The rms position error (or rms integral nonlinearity) is

$$\sigma = \frac{1}{N}\sqrt{\sum_{i=1}^{N}(y_i - x_i)^2} = 14.9\mu m$$

The differential nonlinearity as plotted in Figure 6 is defined in terms of the detector's response function $v(y)$ to uniform irradiation as follows.[10] Let $y = f(x)$ be the track's reconstructed position as a function of the true position x. If the detector is subjected to a uniform irradiation $u(x) = const.$ then

$$v(y) = \frac{1}{f'(x)}$$

is the normalized uniform irradiation response as a function of the reconstructed position y. $f'(x)$ is the derivative of the reconstructed position as a function of the true position. The differential nonlinearity, DFNL, is then defined as:

$$DFNL = \frac{v_{max} - v_{min}}{(v_{max} + v_{min})/2}$$

It can be shown that in terms of the rms position error the DFNL can be written as

$$DFNL = 4\sqrt{2}\pi\sigma/l_a$$

where l_a is the readout node spacing. Applying the above formula we find DFNL=4.8%.

[2]The slits of the collimator were measured to be accurately cut every millimeter with a precision of $\approx$30 microns.

4.4 Choice of the Operating Gas

Threre are three basic requirements that need to be met by a chamber gas suitable for a CSC-based Muon System . These are:

- High drift velocity ($> 60\mu m/nsec$)
- Low ($< 10°$) Lorentz angle
- Nonflammable

Such a gas has been identified and already used for all our tests at the TTR. The composition of the gas is 30% Ar, 50% CO_2, 20% CF_4. Figure 17 shows the drift velocity as a function of electric field for this and two more gases which also meet the requirements. The option of using xenon is being considered if the development of the x-ray alignment system proves to be viable. Figure 18 shows the Lorentz angle as a function of electric-field for the same gases. We expect that the experiment will use one of these gases.

4.5 Tests with cosmic rays at the SSC TTR

Most of the prototypes have been installed at the TTR and have been undergoing tests over the past few months. Figure 19 shows schematically the arrangement of the four small BNL chambers with parallel strips and a two-layer large module. The TTR scintillators in coincidence with a local scintillator and the anode planes are used for triggering. Similar arrangements exist for the rest of the prototypes at the TTR. Figure 20(top) shows a typical Landau distribution from the cathode strips. At the bottom of Figure 20 is shown a spectrum of the highest amplitude of a cluster. The events overflowing the 8-bit FADC are not included in the analysis. Figure 21 shows a typical event as seen by the six cathode planes. The single layer spatial resolution of the small chambers is determined by using three layers to define a track and then histogram the residual of the fourth. Figure 22 shows the distributions of all four of these residuals. Figure 23 shows one of them magnified. Average resolutions over a $\pm 6°$ acceptance in phi are of the order of 68 microns. Figure 24 shows the dependence of the resolution as a function of phi. For normal incidence the resolution is of the order of 45–50 microns. It should be noted that multiple scattering(not subtracted) is estimated to contribute about 30 microns in quadrature. Figure 25 shows the resolution obtained by the 1x1.5 m^2 Dubna prototype. Figure 26 shows the resolutions obtained for nearly normal incidence at three different high voltage values by the Houston group and the 1x0.5 m^2 using Iarocci-type profiles with cathode strips.

The resolution of the full scale prototype is also consistent with <70 microns but is difficult to further quantify it until two more similar layers are available at the end of February. Figure 27 shows a distribution of the quantity ($x_5 - x_6 - h \tan \phi$) The rms should be divided by $\sqrt{2}$ to get the single layer resolution. Further the fact that the transverse coordinate is not known to better than 5 cm contributes an error estimated at about 70 microns which should be subtracted in quadrature. More precise resolution values will be determined when all 4 modules become available. Figure 28 shows the efficiency of the PNPI prototypes. Essentially 100% efficiencies are measured by all the modules tested at the TTR. Figure 29shows the distribution of the earliest time of arrival from the four planes in the PNPI

test setup using 1.7 GeV/c protons from the Gatchina Synchrocyclotron. Constant fraction discriminators were used. It can be seen that all events can be contained in a 16 nsec window.

4.6 Summary

The tests with X-rays described in this report allow a thorough understanding of the cathode strip chambers as well as testing aspects of the technology and our particular design that could be difficult or impossible to be performed in a single layer setup either with cosmic rays or beam particles. The capacitive interpolation with the floating strips, its effects on resolution and differential nonlinearity are examples of the latter. We have demonstrated a compact, low cost, multiplexed readout suitable for systems with large numbers of channels. The 288 channels of this prototype represent nearly one third of the maximum number of channels anticipated for *any* GEM superlayer module. Noise levels of 1600 equivalent rms electrons for 550 nsec shaping time has been demonstrated. Intercalibration of the cathode strip channels to the 0.5% level has been achieved. Gas amplification stability and its implications to construction tolerances have been thoroughly studied. The capacitive interpolation with the floating strips has been found to perform as designed both in restoring linear response and in reducing the capacitive load of the preamplifiers. Finally the achieved resolution of $\approx 50\mu m$ is consistent with the limits imposed by the range of photoelectrons indicating no other fundamental limits due to excessive thermal noise etc. Tests with cosmic rays show single layer resolution consistent with the baseline design, demonstrate fully efficient bunch crossing tagging, and operation with a safe gas suitable for use in the GEM Detector. Noise and calibration issues were demonstrated with a large number of channels.

References

[1] E. Gatti, A. Longoni, H. Okuno, and P. Semenza, Nucl. Instr. and Meth. **163**, 83, (1979).

[2] V. Radeka, and R.A. Boie, Nucl. Instr. and Meth. **178**, 543, (1980).

[3] E. Gatti, A. Longoni, and V. Radeka, Nucl. Instr. and Meth. **220**, 445, (1984).

[4] E. Mathieson, and G.C. Smith, IEEE Transactions on Nuclear Science, Vol. 36, No. 1, February 1989.

[5] B. Yu, G.C. Smith, and V. Radeka, "Developments in interpolating cathode structures for high precision gas proportional detectors", to be presented at the 1992 IEEE Nuclear Science Symposium, Orlando, Florida, 1992.

[6] J. Fischer, V. Radeka, and G.C. Smith, Nucl. Instr. and Meth. **A252**, 239, (1986).

[7] "AMPLEX-A Low noise, Low power Analog CMOS Signal Processor for Multielement Silicon Particle Detectors", E. Beuville, K. Borer, E. Chesi, EHM Heijne, P. Jarron, B. Lisowski, S. Singh, CERN/EF89-9, Sept. 1989.

[8] E. Chesi. and P. Martinengo. "Digital Readout for Analog. Multiplexed Signals", CERN, Note PS 202, January 1988.

[9] "The GEM Muon System Based on Cathode Strip Chambers, GEM TN-92-199, October,1992.

[10] B. Yu,"Gas Proportional Detectors with Interpolating Cathode Pad Readout for High Track Multiplicities", Ph.D. Thesis, Pittsburgh 1991 (BNL 47055 Informal Report).

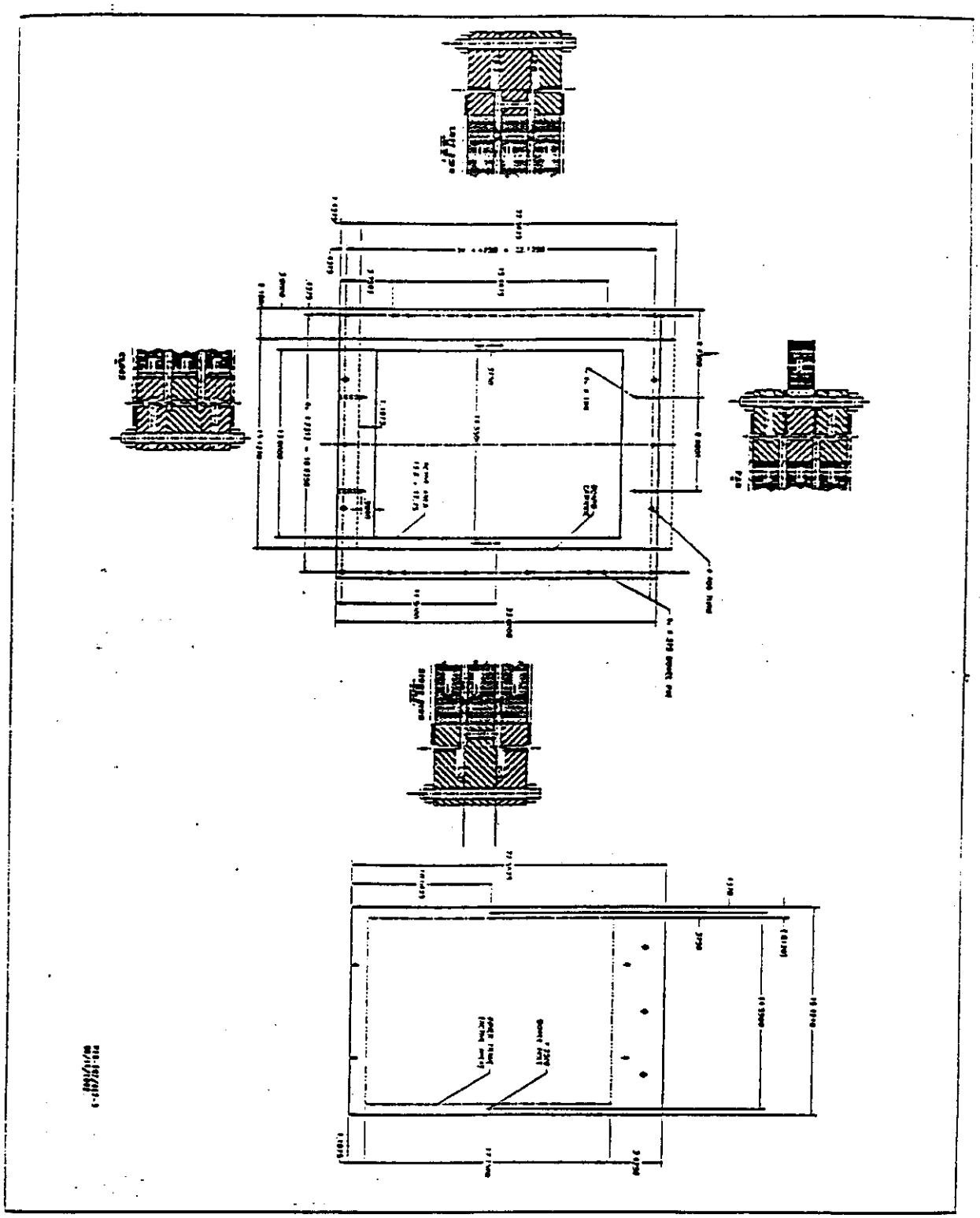

Figure 1

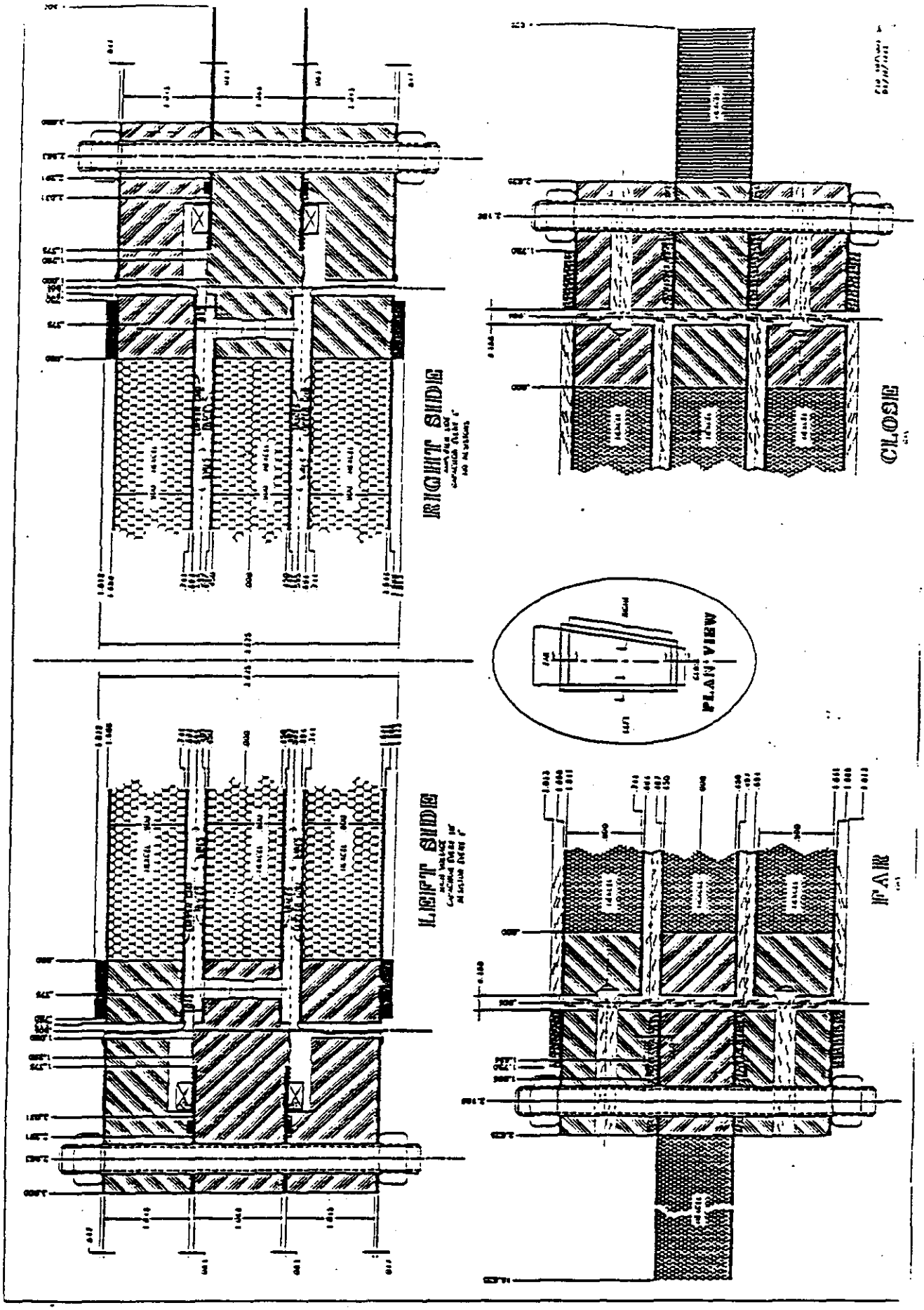

Figure 2

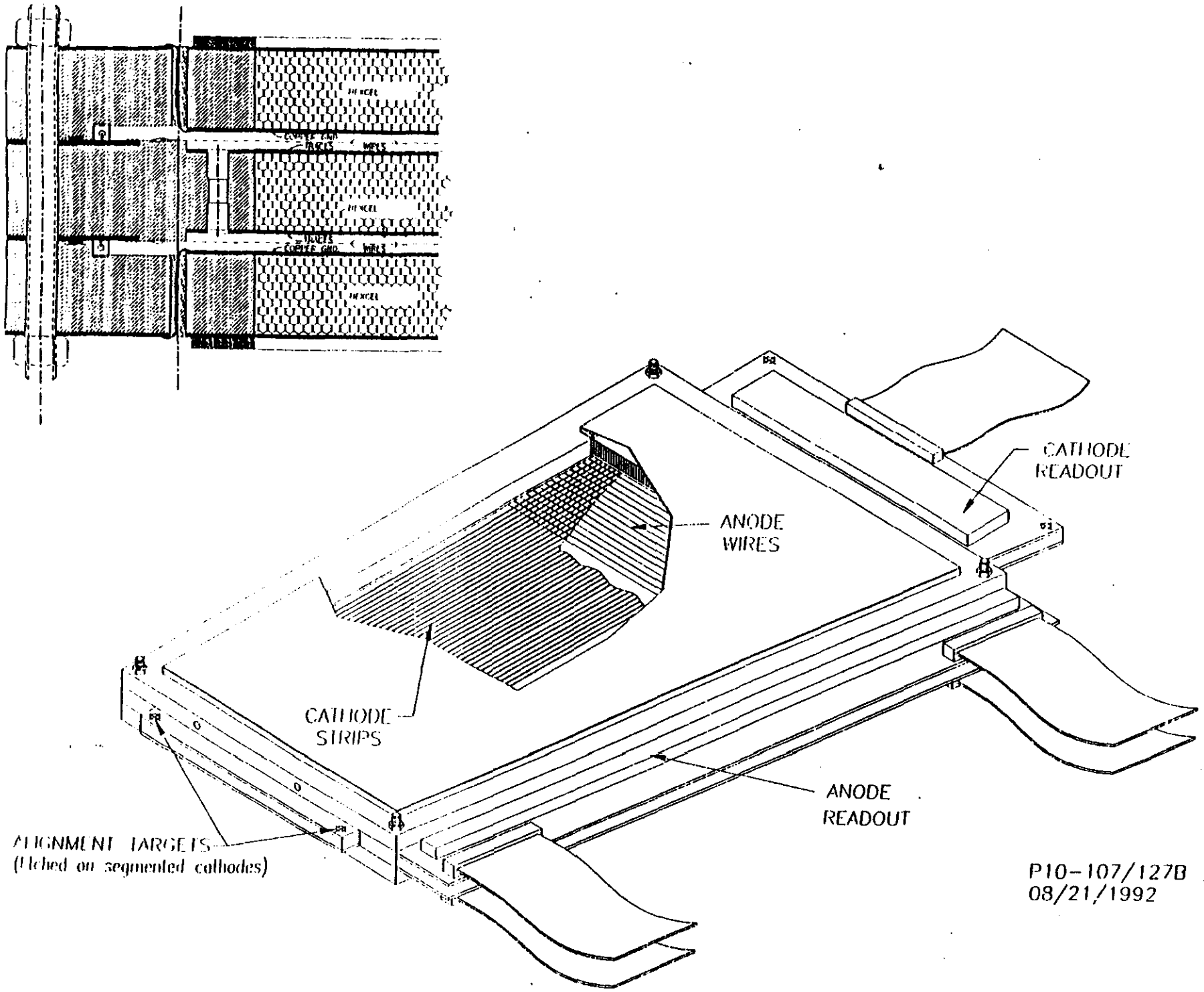
CATHODE READOUT
ANODE WIRES
CATHODE STRIPS
ANODE READOUT
ALIGNMENT TARGETS
(Etched on segmented cathodes)
P10-107/127B
08/21/1992

Figure 3

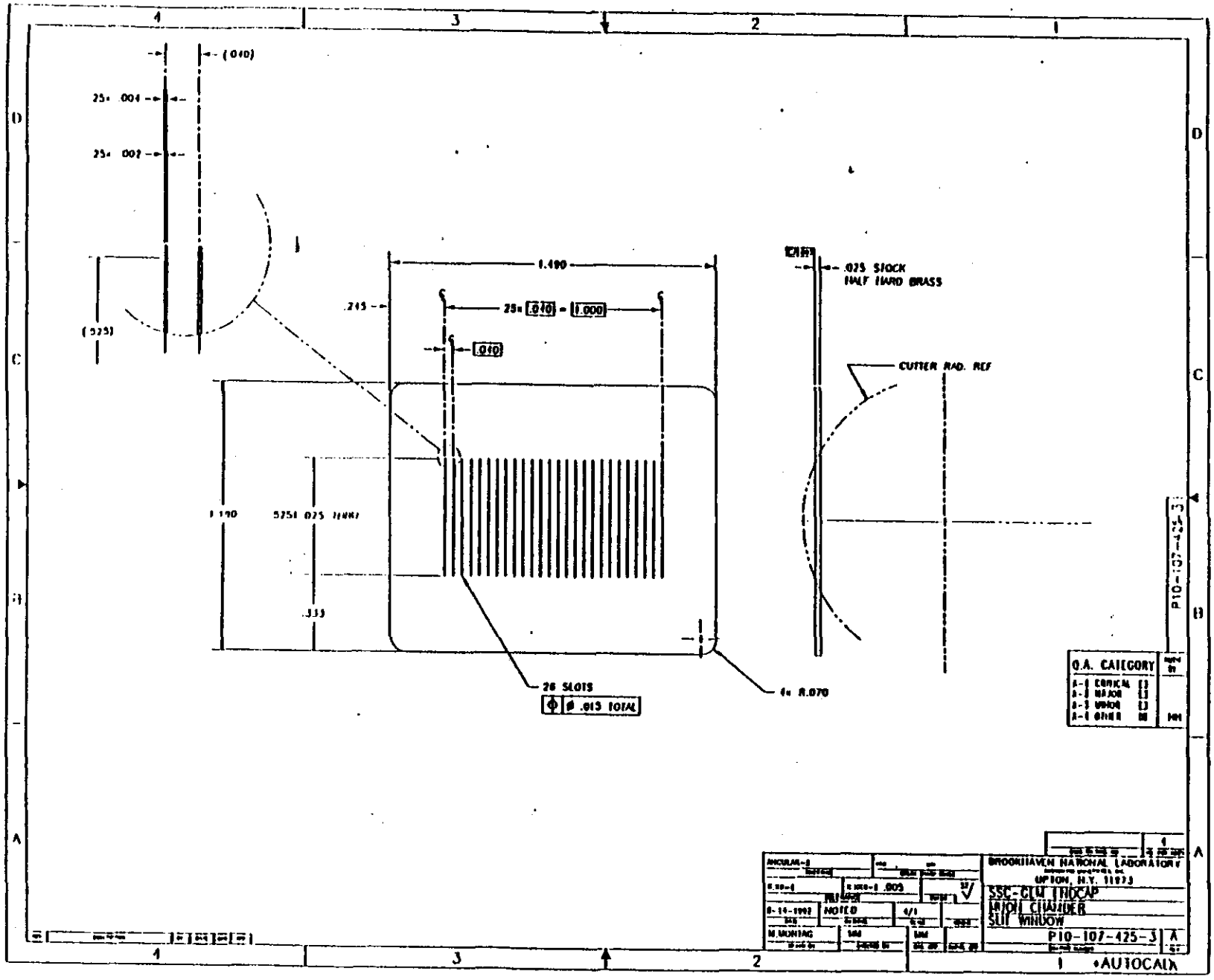

(.040)
25x .004
25x .002
(.525)
1.490
.245
25x .040 = 1.000
.040
.025 STOCK
HALF HARD BRASS
CUTTER RAD. REF
1.190
.525±.025 (HHR)
.333
26 SLOTS
Φ .015 TOTAL
4x R.070
Q.A. CATEGORY
A-1 CRITICAL
A-2 MAJOR
A-3 MINOR
A-4 OTHER
BROOKHAVEN NATIONAL LABORATORY
UPTON, N.Y. 11973
SSC-GEM ENDCAP
MUON CHAMBER
SLIT WINDOW
P10-107-425-3
A
NOTED
M.MONTAG
AUTOCAD

Figure 4

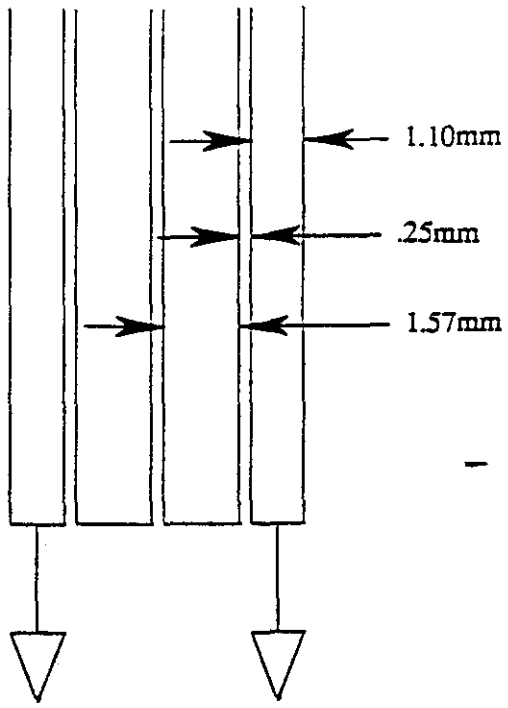

Figure 5a

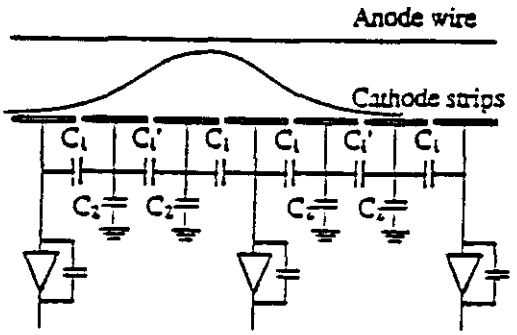

Figure 5b

op_varw1

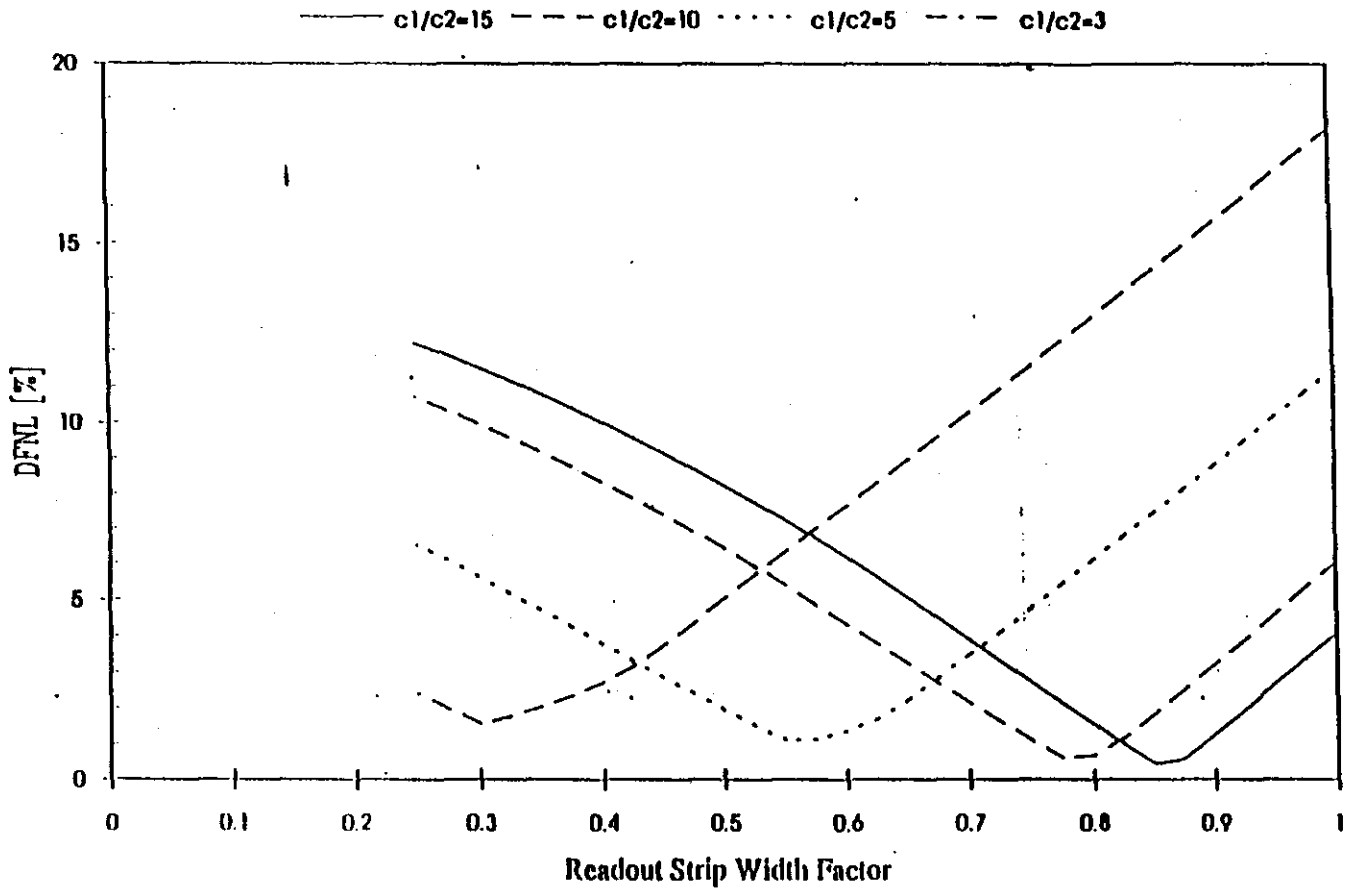

Figure 6

la=5, h=2.5, k3=.55, width factor is calculated with respect to la/3

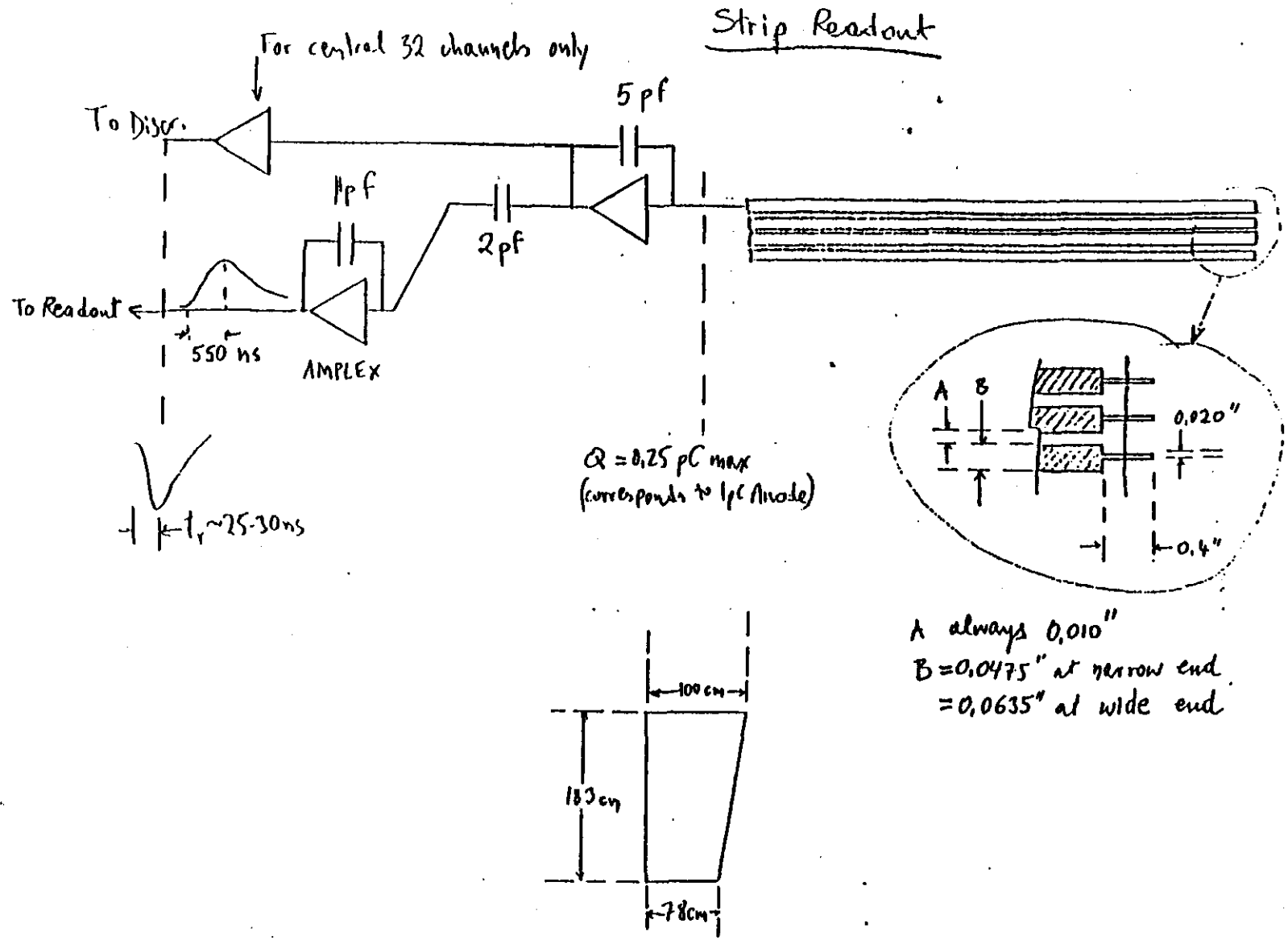
Strip Readout
For central 32 channels only
To Discr.
5 pf
1pf
2pf
To Readout
550 ns
AMPLEX
t_r ~25-30ns
Q = 0.25 pC max
(corresponds to 1pC Anode)
A
B
0.020"
0.4"
A always 0.010"
B = 0.0475" at narrow end
= 0.0635" at wide end
100 cm
183 cm
78cm

Figure 7

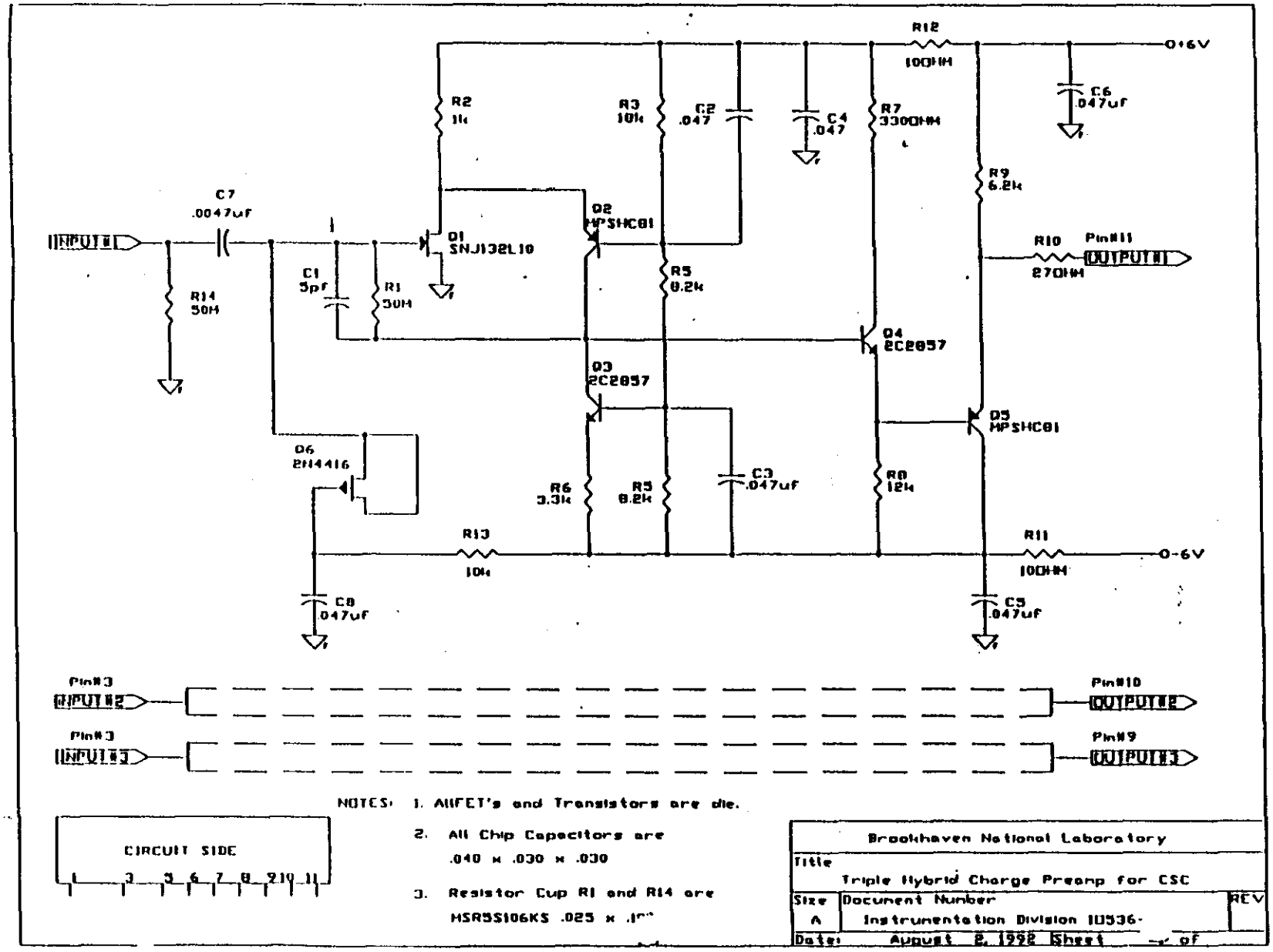
INPUT#1
C7
.0047uf
R14
50M
C1
5pf
R1
50M
R2
1k
D1
SNJ132L10
D2
MPSHC01
R3
10k
C2
.047
C4
.047
R12
100HM
+6V
C6
.047uf
R7
330OHM
R9
6.2k
R10
270HM
Pin#11
OUTPUT#1
R5
8.2k
D4
2C2857
D3
2C2857
D5
MPSHC01
D6
2N4416
R6
3.3k
R3
8.2k
C3
.047uf
R8
12k
R13
10k
R11
100HM
-6V
C8
.047uf
C5
.047uf
Pin#3
INPUT#2
Pin#10
OUTPUT#2
Pin#3
INPUT#3
Pin#9
OUTPUT#3
CIRCUIT SIDE
1 3 5 6 7 8 9 10 11
NOTES: 1. All FET's and Transistors are die.
2. All Chip Capacitors are .040 x .030 x .030
3. Resistor Cup R1 and R14 are HSR5S106KS .025 x .1"
Brookhaven National Laboratory
Title
Triple Hybrid Charge Preamp for CSC
Size
A
Document Number
Instrumentation Division 10536-
REV
Date: August 2, 1992 Sheet of

Figure 8

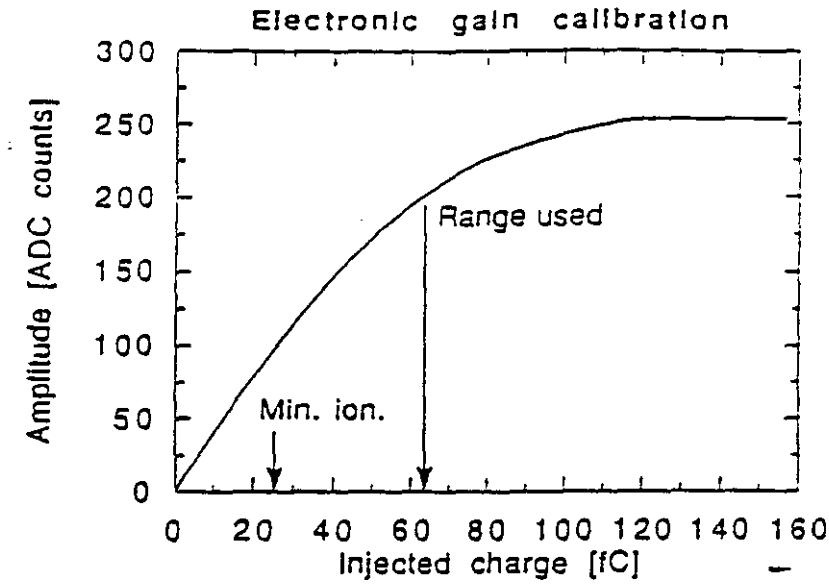

Figure 9a

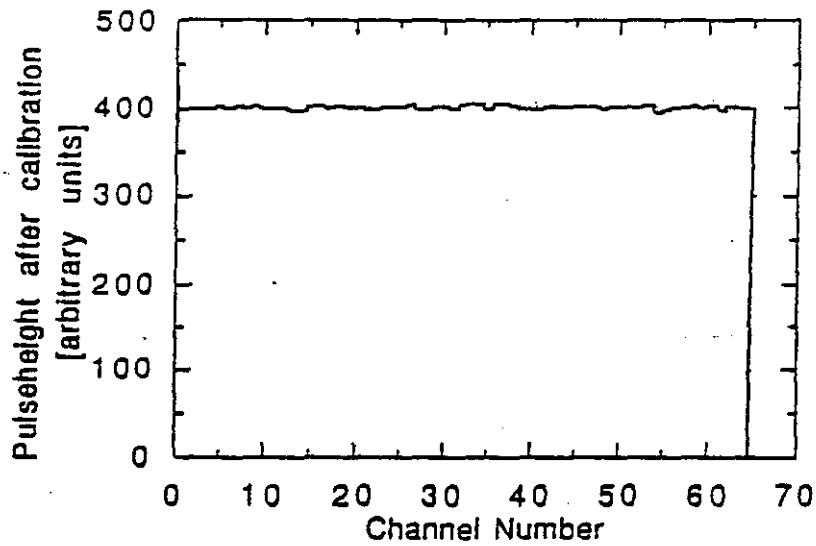

Figure 9b

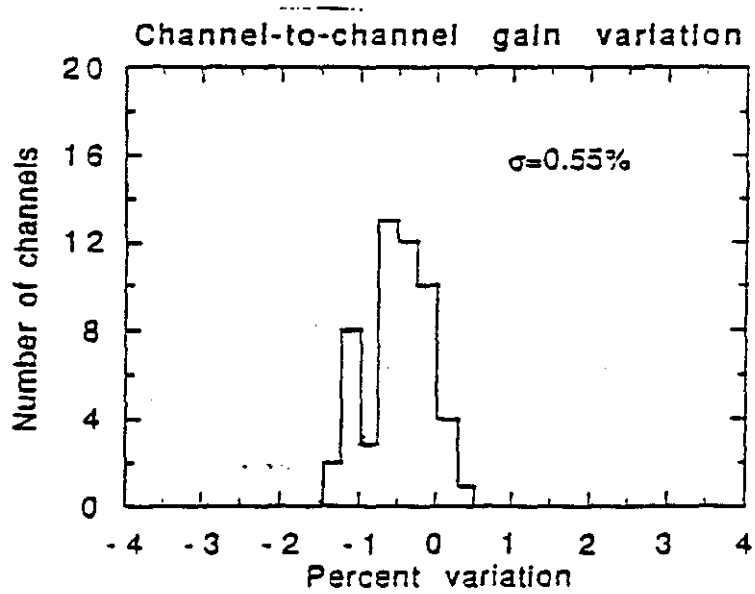

Figure 9c

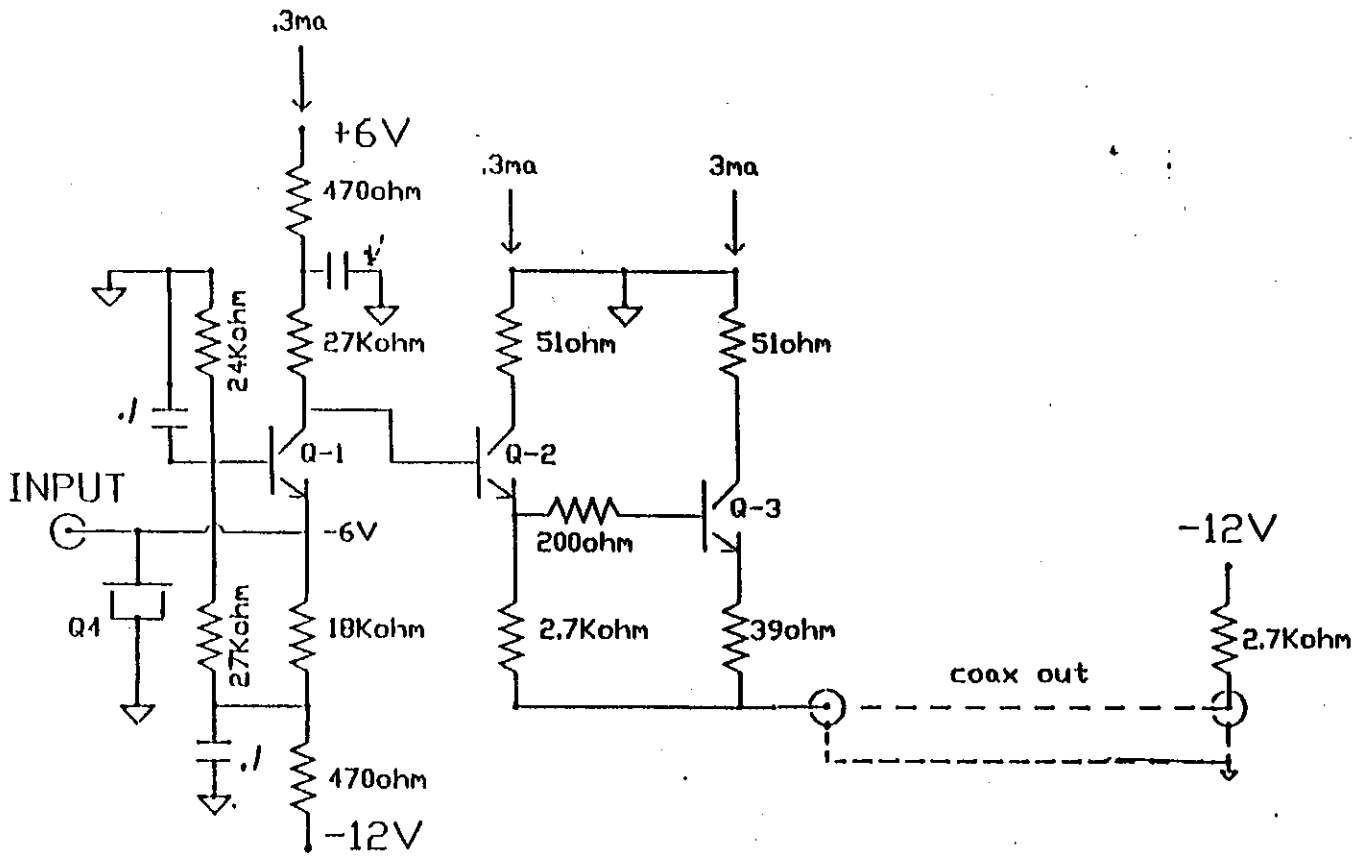

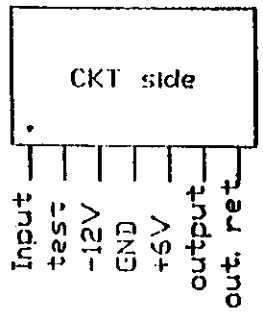

Q1-BFT-25
Q2-BFT-25
Q3-BFR-92
Q4-2N4416/FET

preamplifier Dim .700"x.400"
pins on .100" CC.
pin #1-*

Figure 10

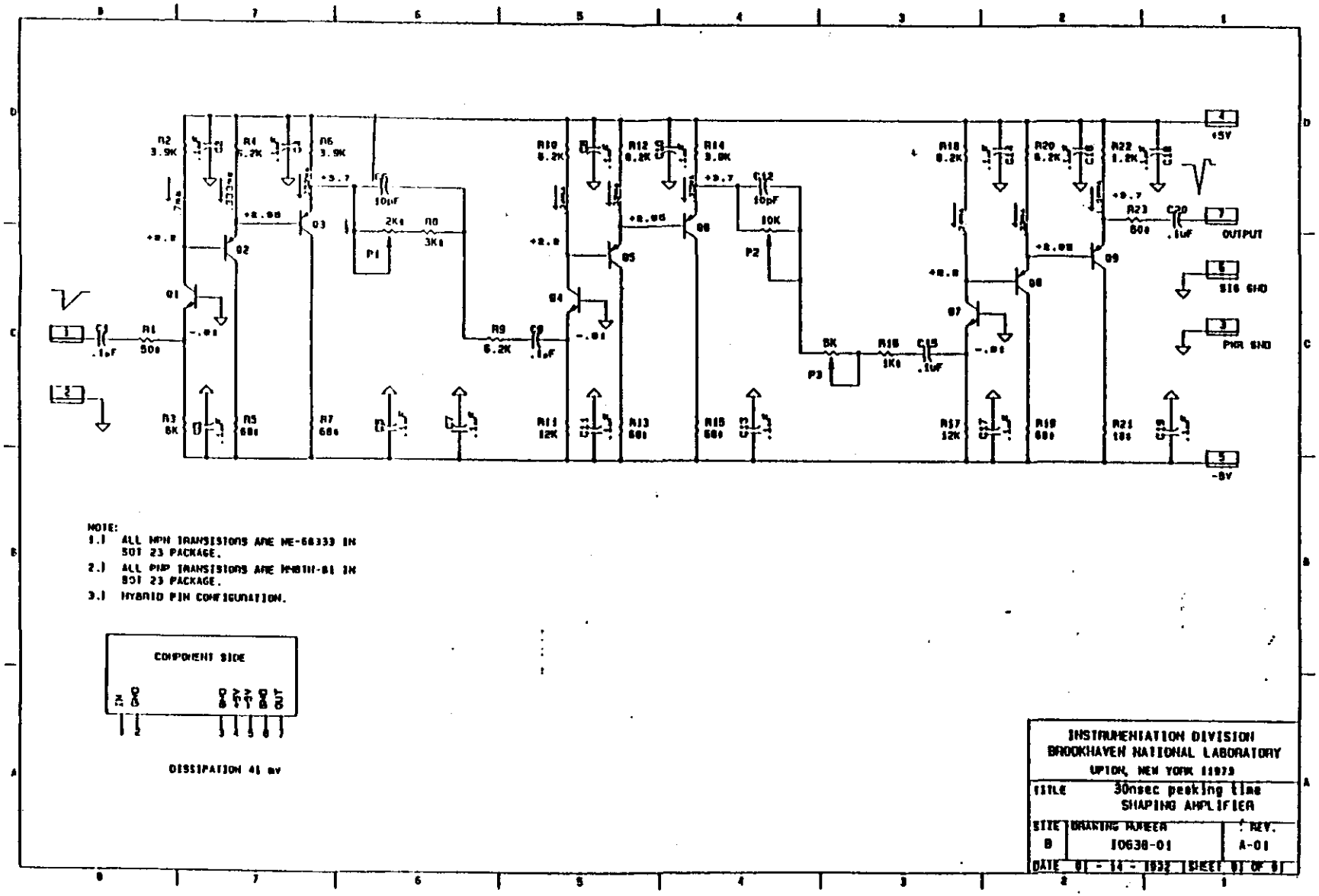
NOTE:
1.) ALL NPN TRANSISTORS ARE NE-68333 IN SOT 23 PACKAGE.
2.) ALL PNP TRANSISTORS ARE MMBTH-81 IN SOT 23 PACKAGE.
3.) HYBRID PIN CONFIGURATION.
COMPONENT SIDE
DISSIPATION 41 mv
INSTRUMENTATION DIVISION
BROOKHAVEN NATIONAL LABORATORY
UPTON, NEW YORK 11973
TITLE 30nsec peaking time SHAPING AMPLIFIER
SIZE B
DRAWING NUMBER 10638-01
REV. A-01
DATE 8 - 14 - 1992
SHEET 8 OF 8
+5V
OUTPUT
SIG GND
PWR GND
-5V

Figure 11

1/7/93 Preliminary IC6ANOIS.XLS 2:32 PM

IC6A	Device #7		Qin:	5.00E-14					1/7/93
Cd	Vout	Vnoise	System	SNR	Gain	ENC	ENC	Slope	Intercept
0	1.839	6.18	0.65	299	36.78	1.67E-16	1043	6.85	1018.85
22	1.771	6.7	0.96	267	35.42	1.87E-16	1168		
47	1.697	7.13	0.64	239	33.94	2.09E-16	1306		
68	1.613	7.75	0.94	210	32.26	2.38E-16	1488		
100	1.485	8.13	0.74	183	29.70	2.73E-16	1701		
150	1.377	9.13	0.94	152	27.54	3.30E-16	2058		
pF	V p-p	mV rms	mV rms	-	mV/fC	C	e-	e-/pF	e-

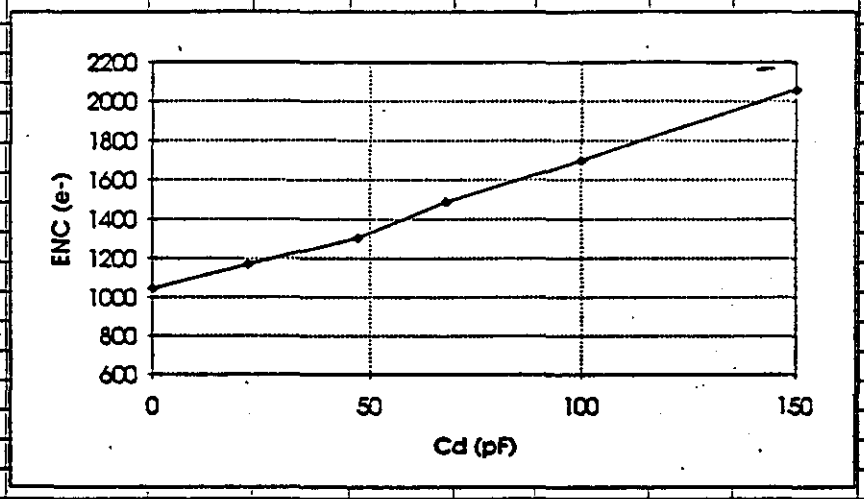

1/7/93 IC6ANOIS.XLS 2:32 PM

Linearity									
	Cd=100 pF			Tp=750 nsec					1/7/93
Vin	Vout								
0	0								
25	734								
50	1506								
100	2946								
140	3806								
150	4020								
160	4201								
170	4351								
180	4481								
200	4700								

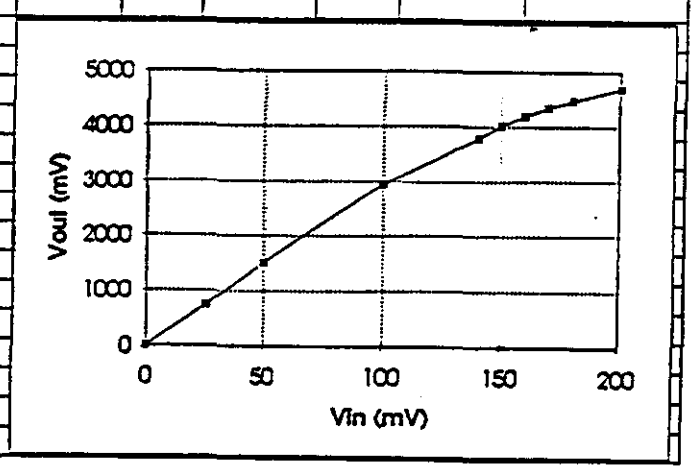

Gas amplification uniformity (%)

Chamber 2B

1.1	10.1	-9.8	4.7	-8.0	-9.8	-8.0	-13.4
6.4	10.1	-4.4	8.3	1.1	-8.0	-4.4	-15.2
10.1	8.3	-6.2	4.7	1.1	-6.2	-8.0	-13.4
17.3	17.3	-4.4	17.3	13.7	-4.4	-4.4	-15.2
6.4	10.1	-4.4	11.9	4.7	-4.4	-4.4	-11.6

Figure 12a

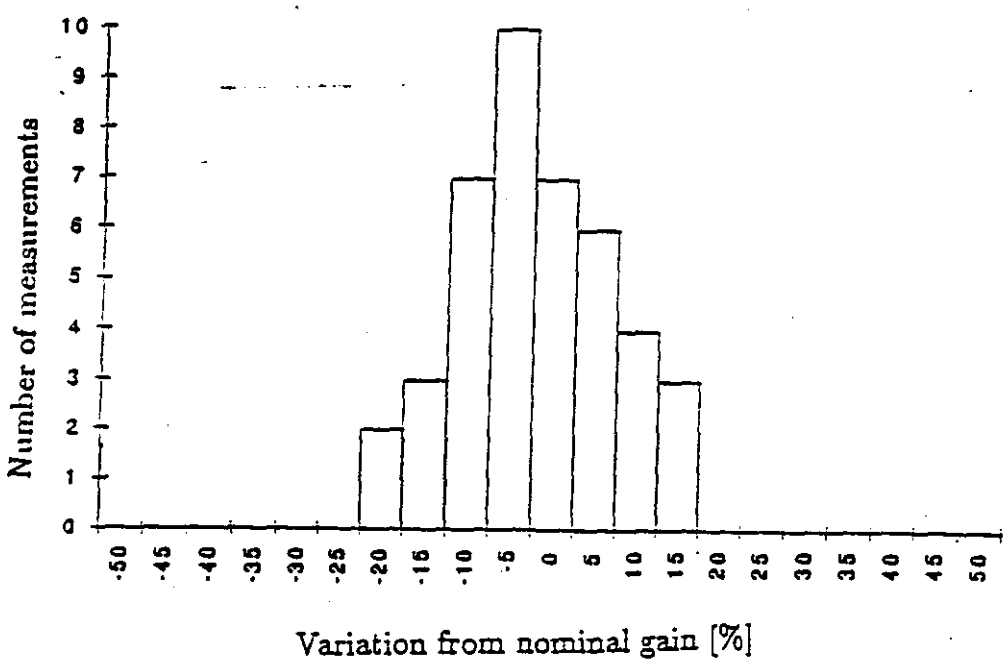

Figure 12b

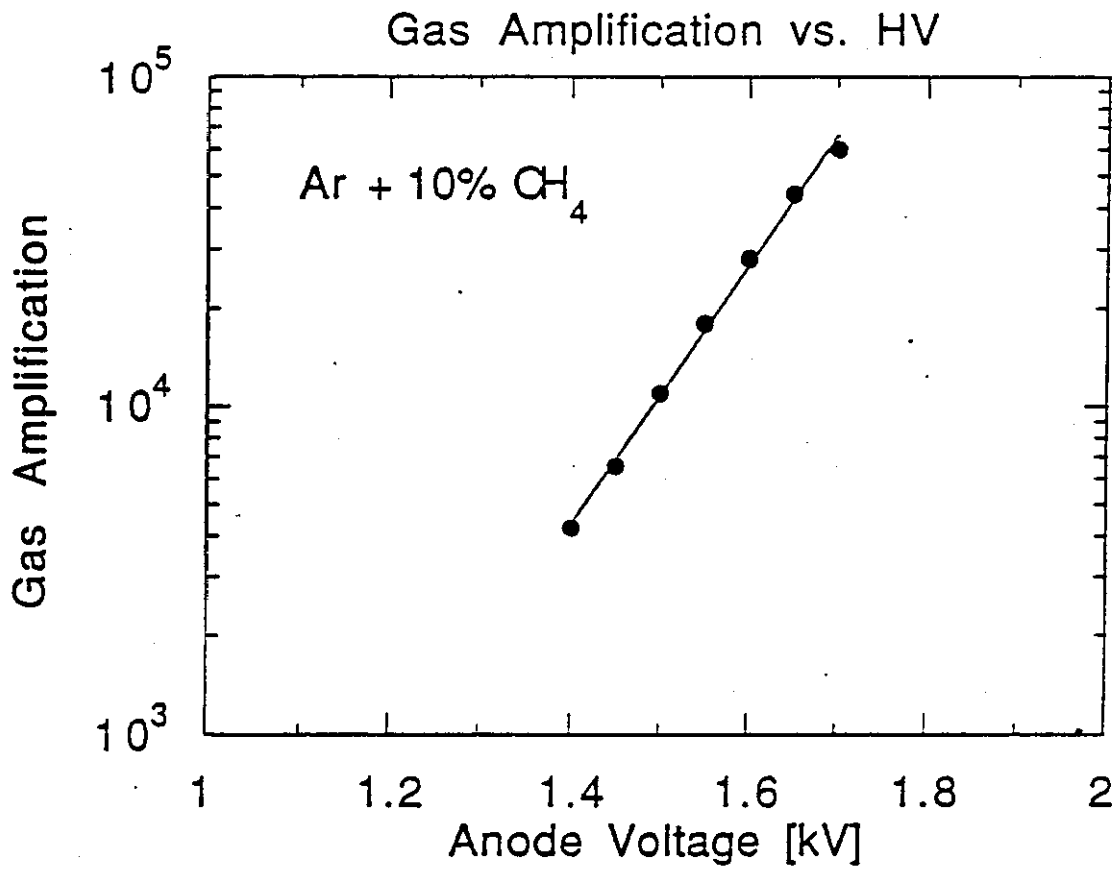
Gas Amplification vs. HV
Ar + 10% CH4
Gas Amplification
10^5
10^4
10^3
1
1.2
1.4
1.6
1.8
2
Anode Voltage [kV]

Figure 13

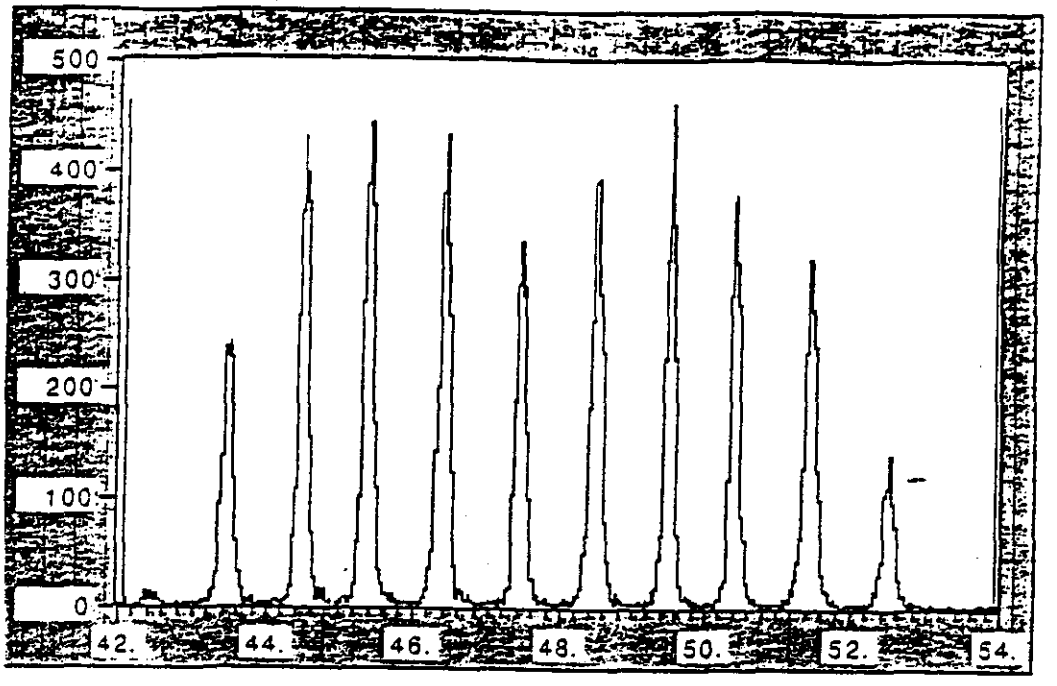

Figure 14a

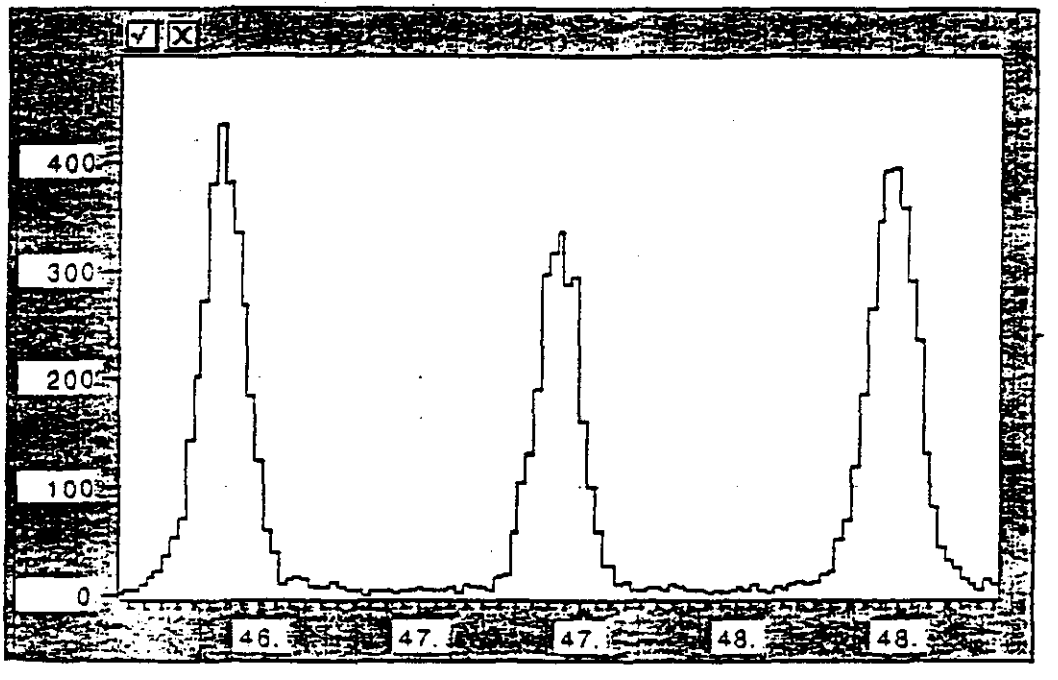

Figure 14b

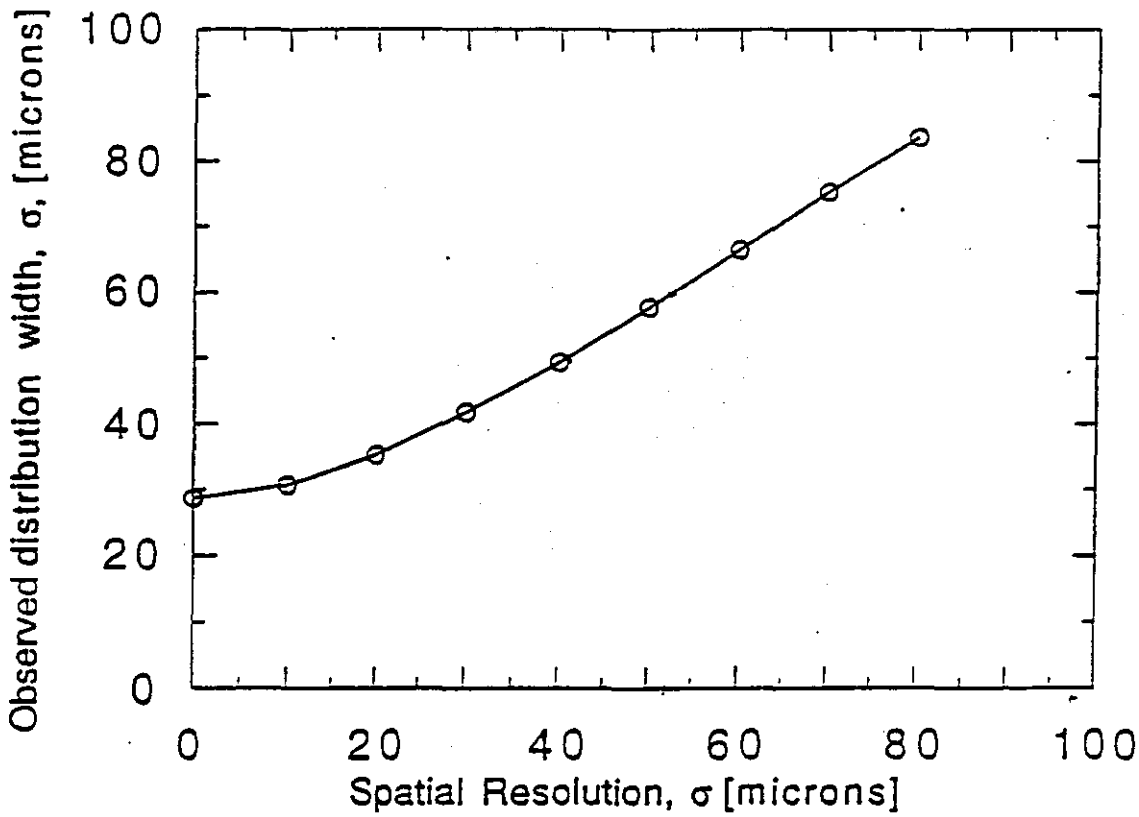
Observed distribution width, σ, [microns]
100
80
60
40
20
0
0
20
40
60
80
100
Spatial Resolution, σ [microns]

Figure 15

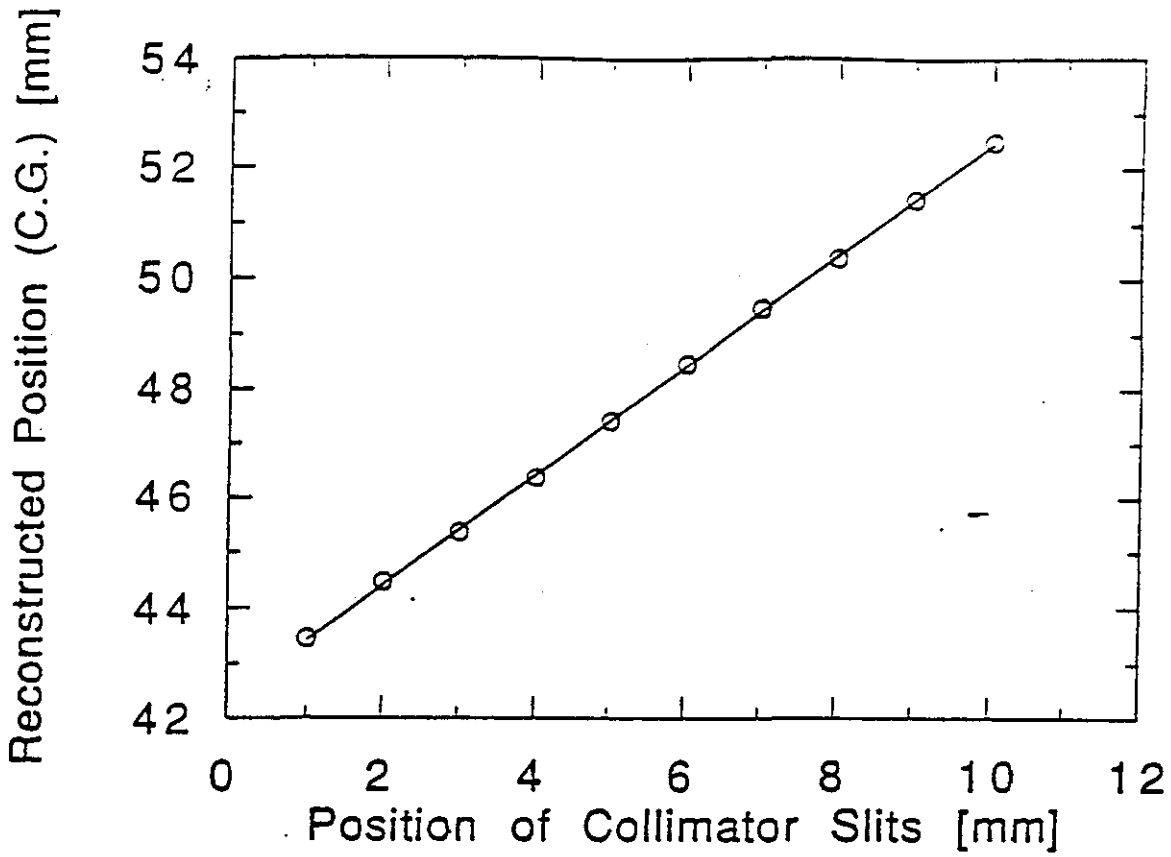

Figure 16a

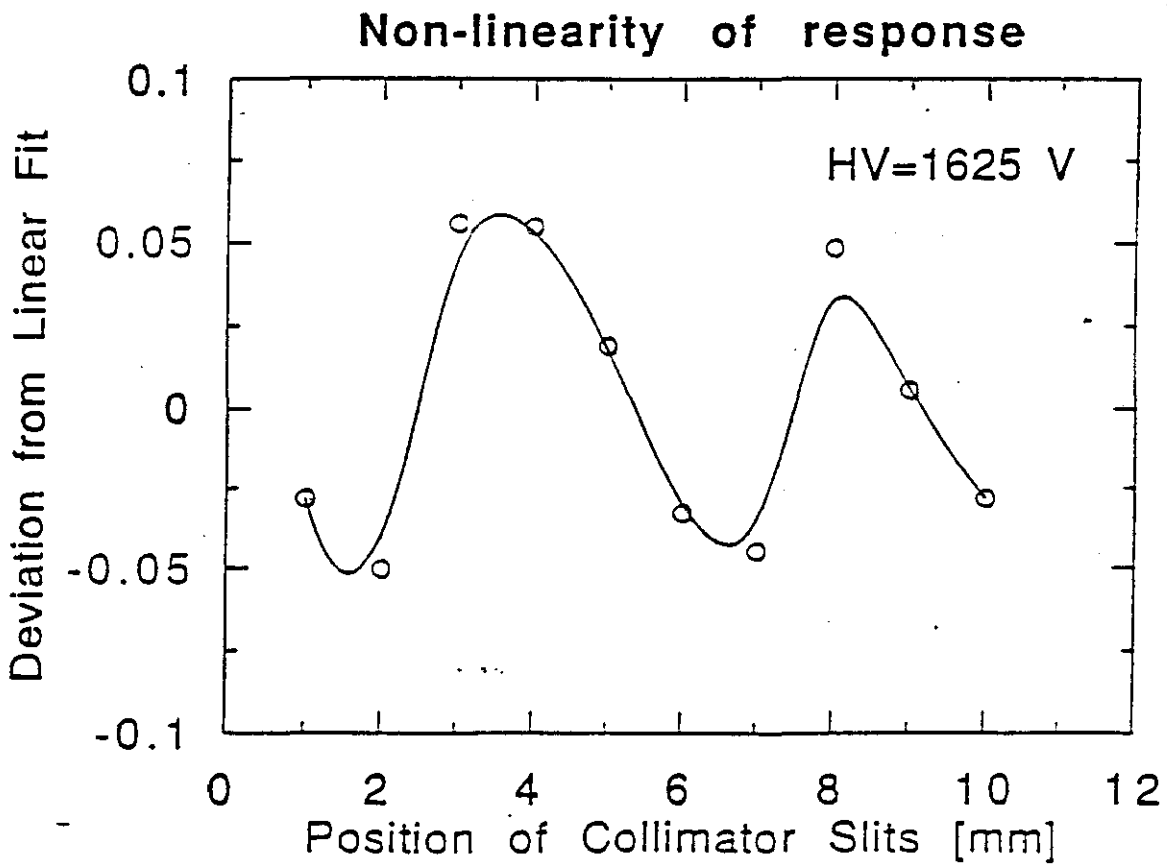

Figure 16b

Drift velocity

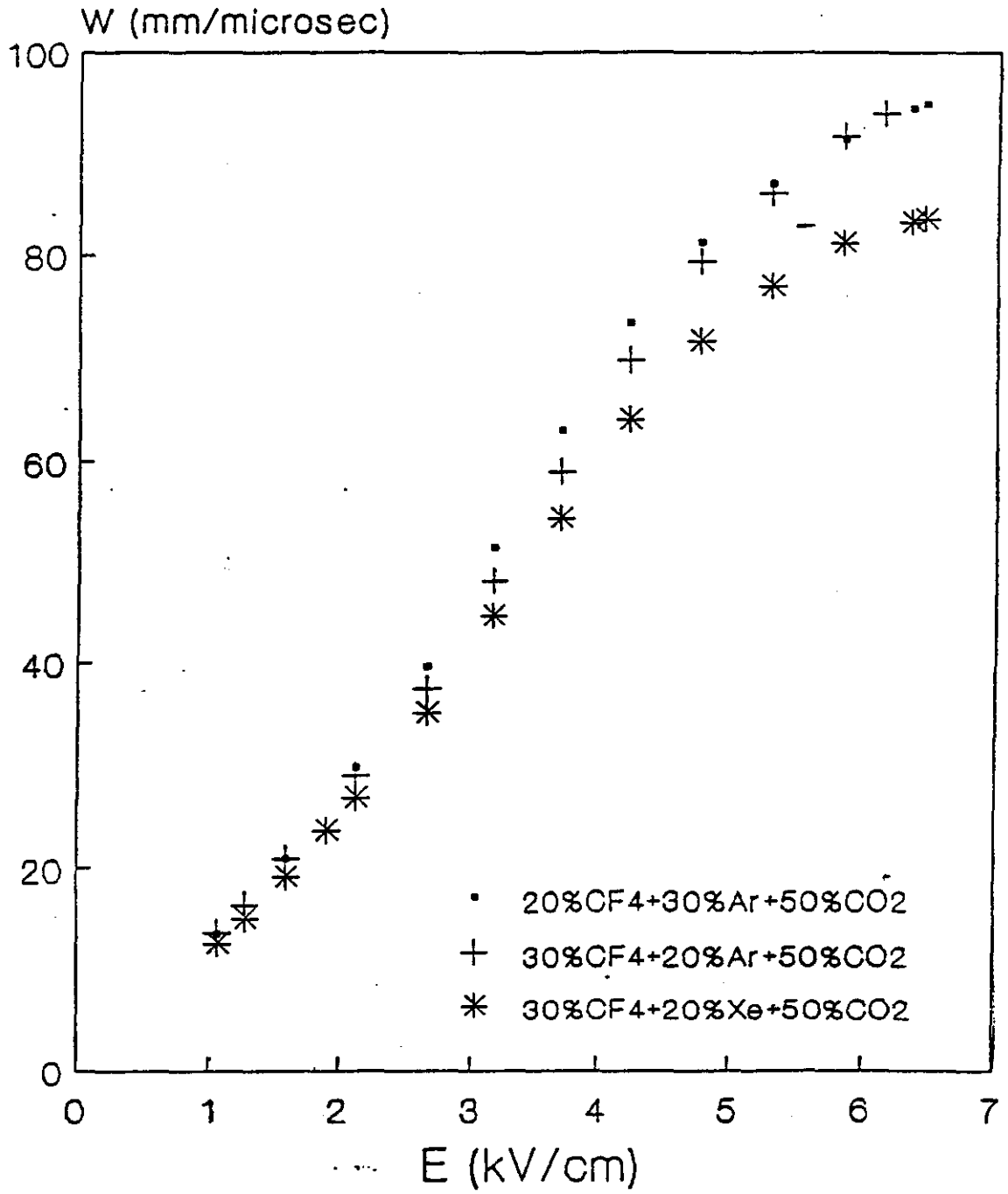

Fig. 17

Lorentz angle
B = 0.8 T

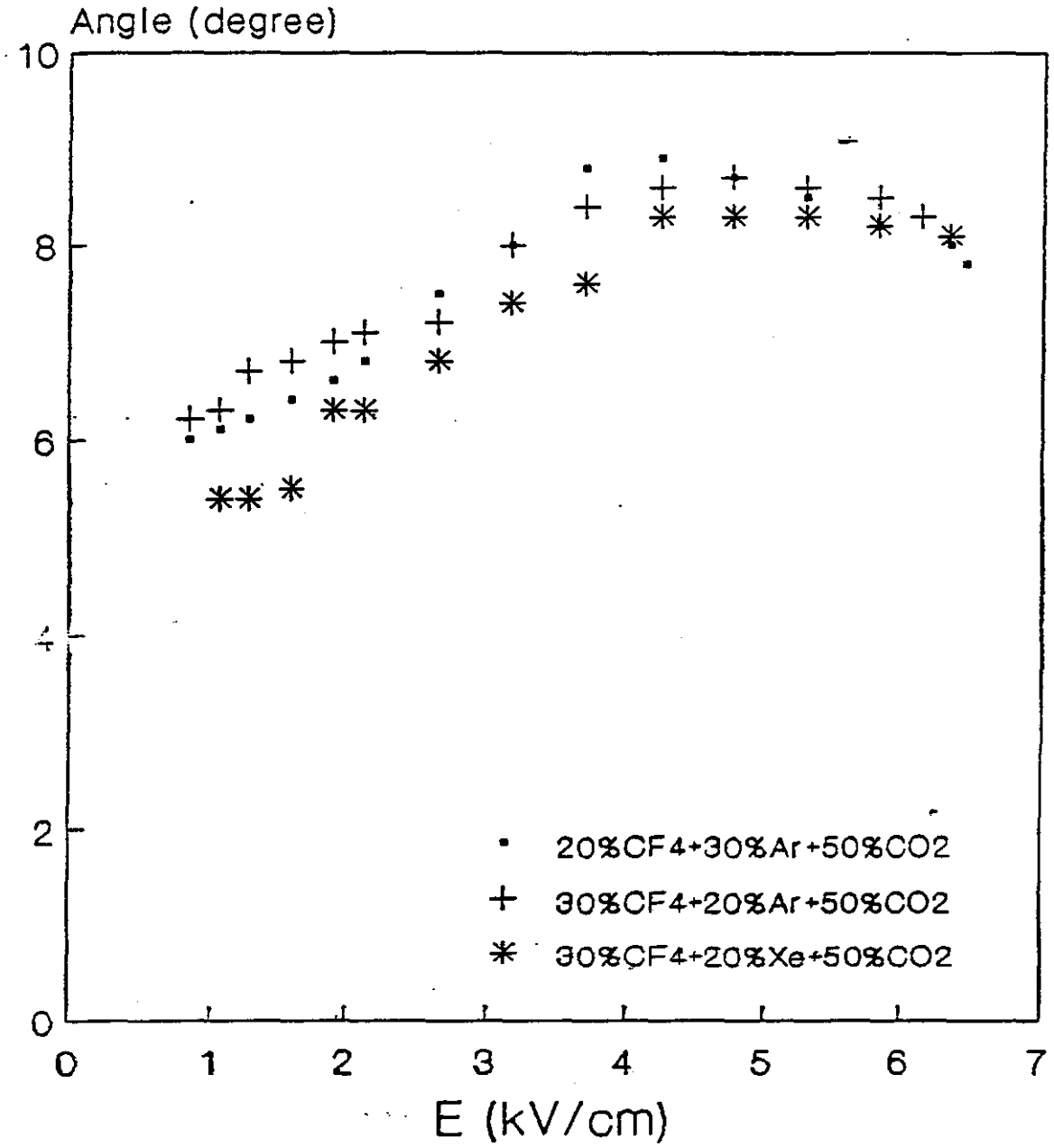

Fig. 18

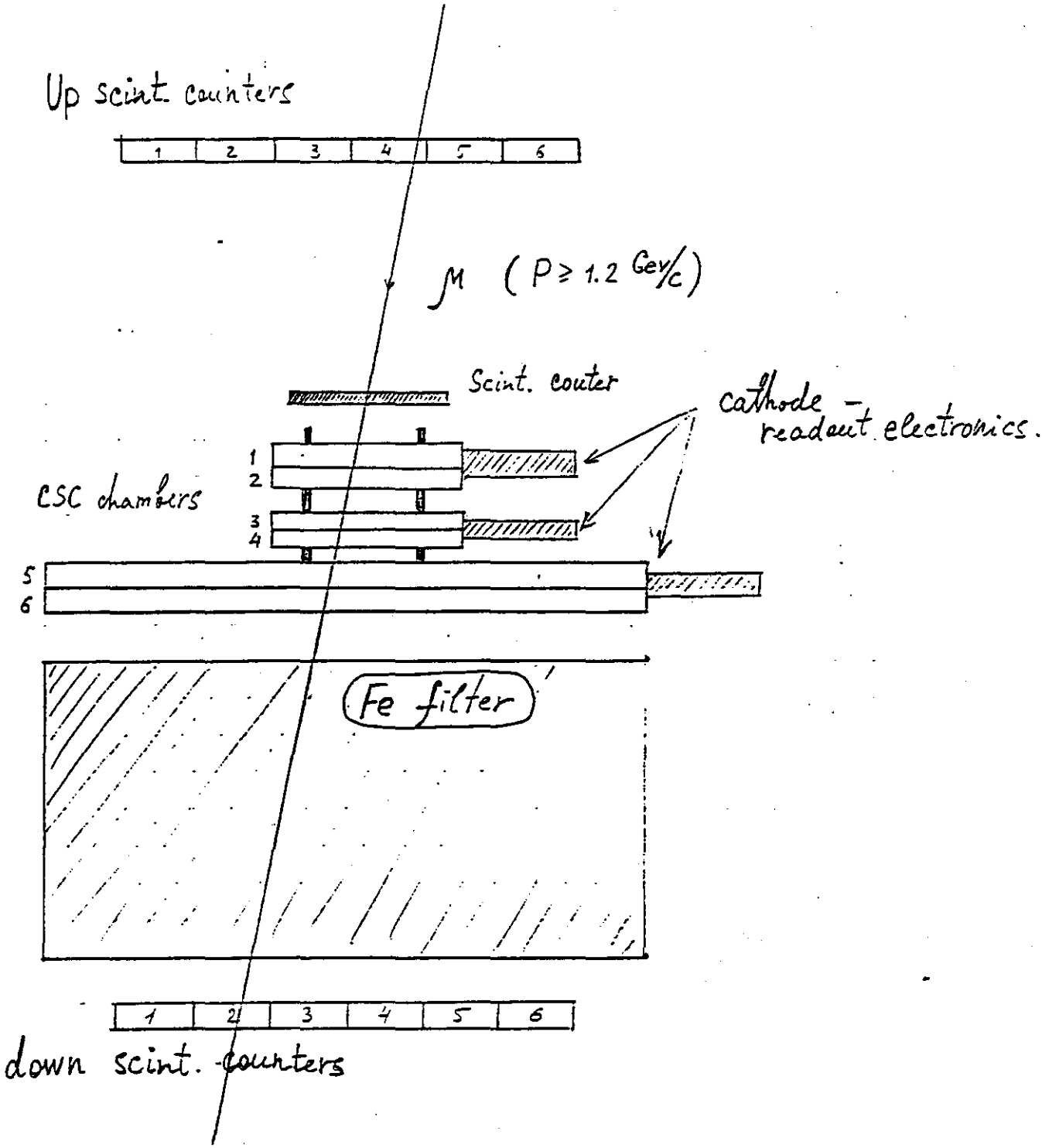
Up scint. counters
1
2
3
4
5
6
μ (P ≥ 1.2 Gev/c)
Scint. couter
cathode - readout electronics.
CSC chambers
1
2
3
4
5
6
Fe filter
1
2
3
4
5
6
down scint. counters

Fig 19

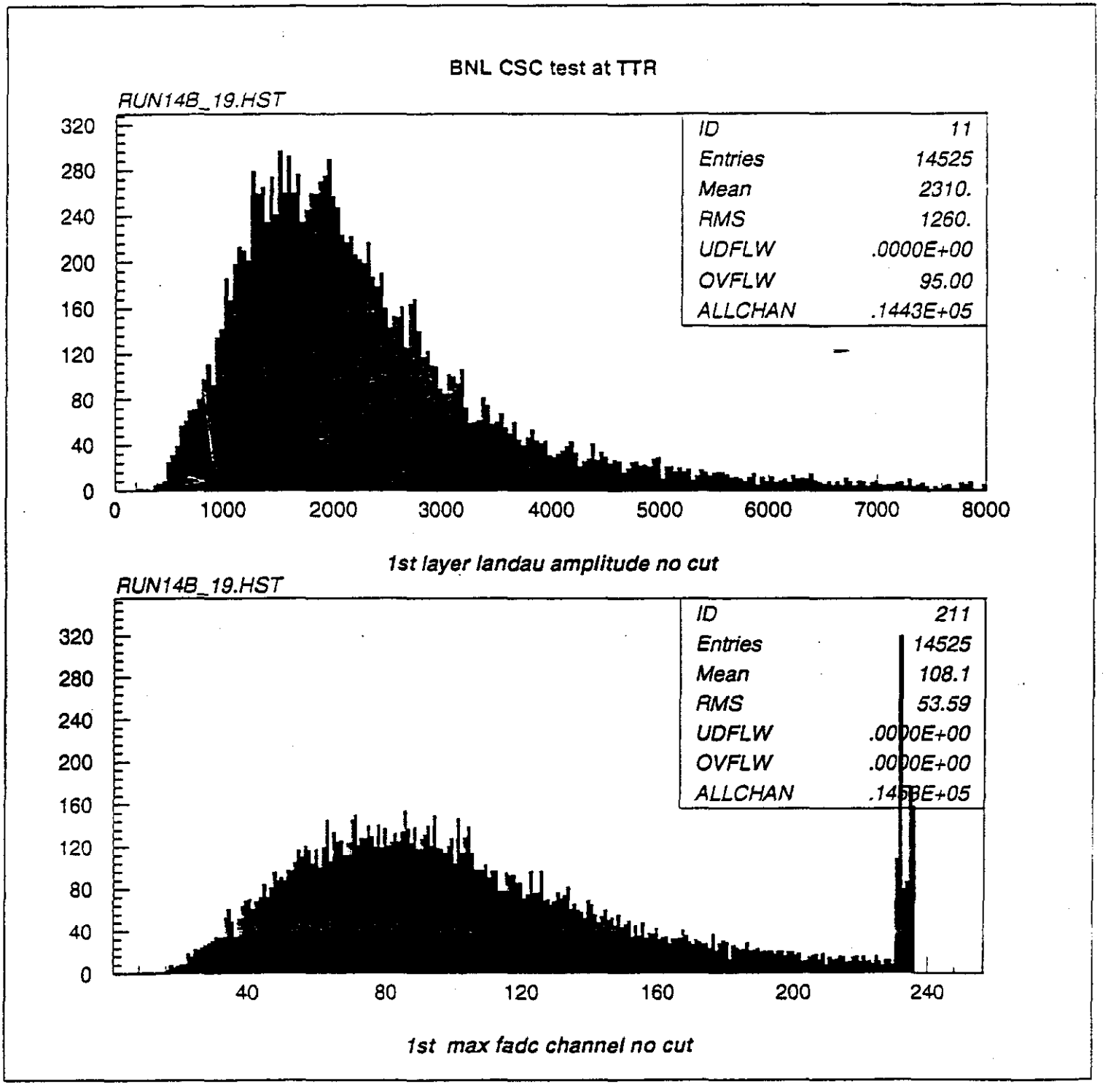
BNL CSC test at TTR
RUN14B_19.HST
ID 11
Entries 14525
Mean 2310.
RMS 1260.
UDFLW .0000E+00
OVFLW 95.00
ALLCHAN .1443E+05
320
280
240
200
160
120
80
40
0
0
1000
2000
3000
4000
5000
6000
7000
8000
1st layer landau amplitude no cut
RUN14B_19.HST
ID 211
Entries 14525
Mean 108.1
RMS 53.59
UDFLW .0000E+00
OVFLW .0000E+00
ALLCHAN .1456E+05
320
280
240
200
160
120
80
40
0
40
80
120
160
200
240
1st max fadc channel no cut

Fig 20

Front Panel

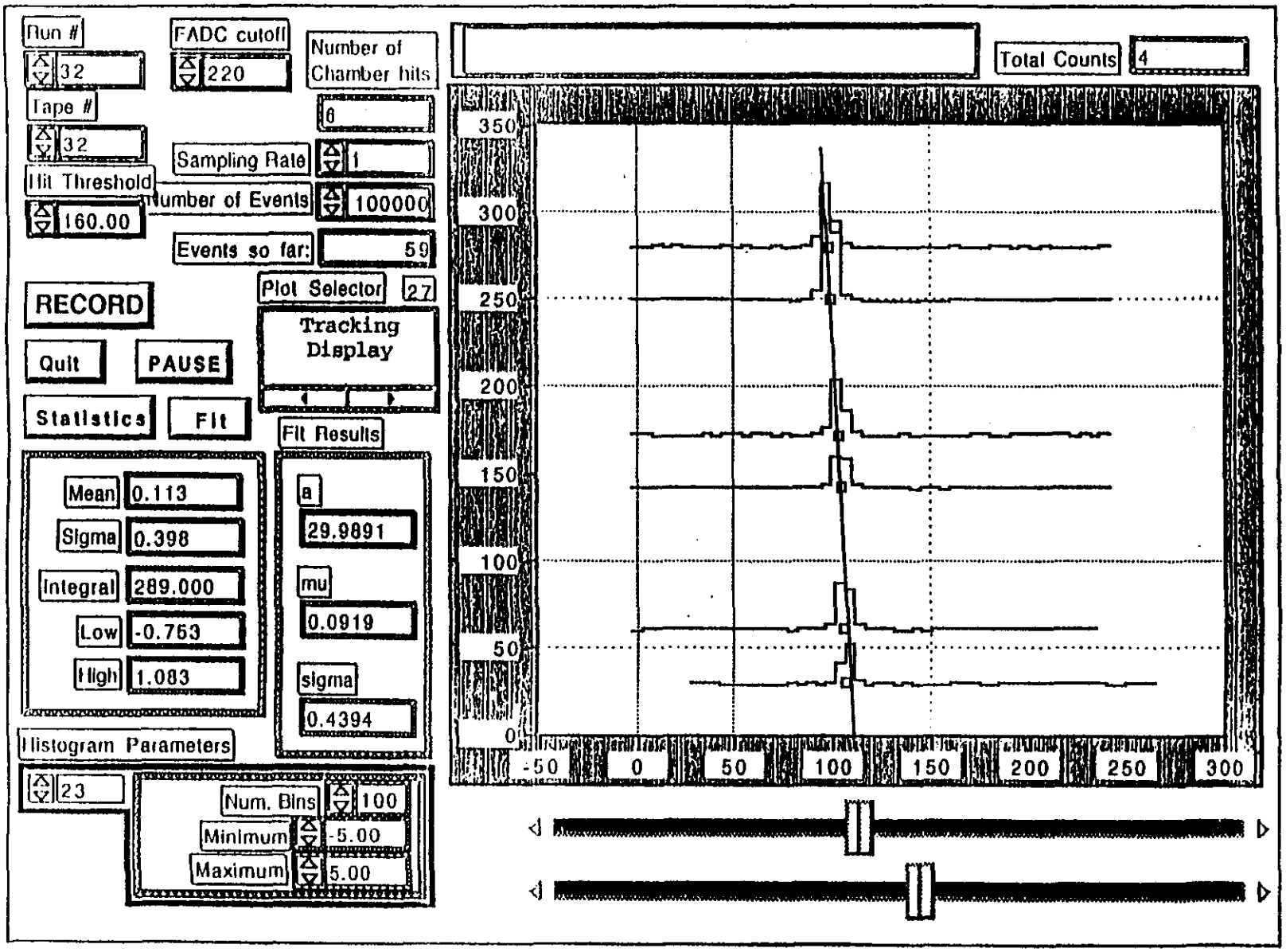

Fig 21

BNL CSC test at TTR

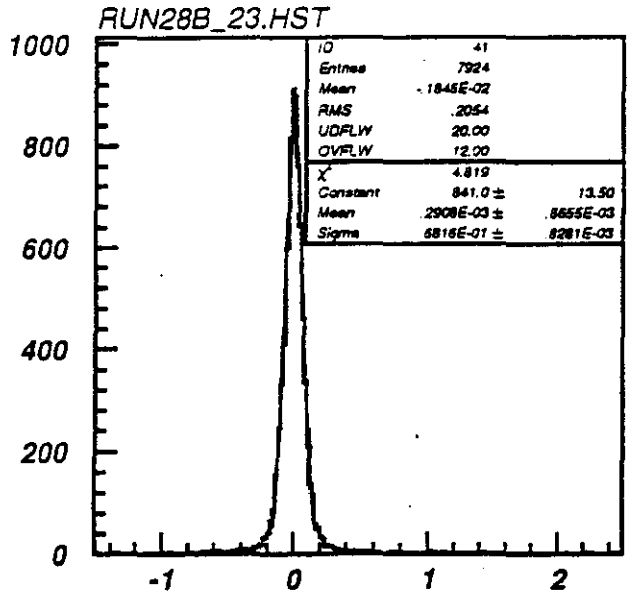

1st layer residuals +/- 6 deg

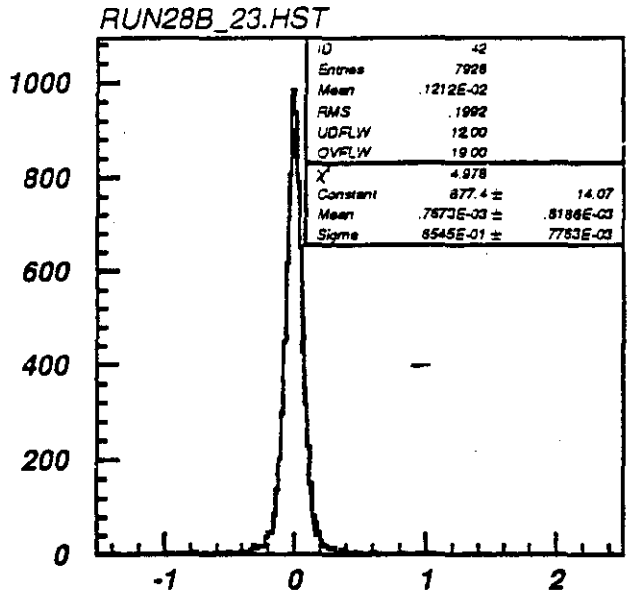

2nd layer residuals +/- 6 deg

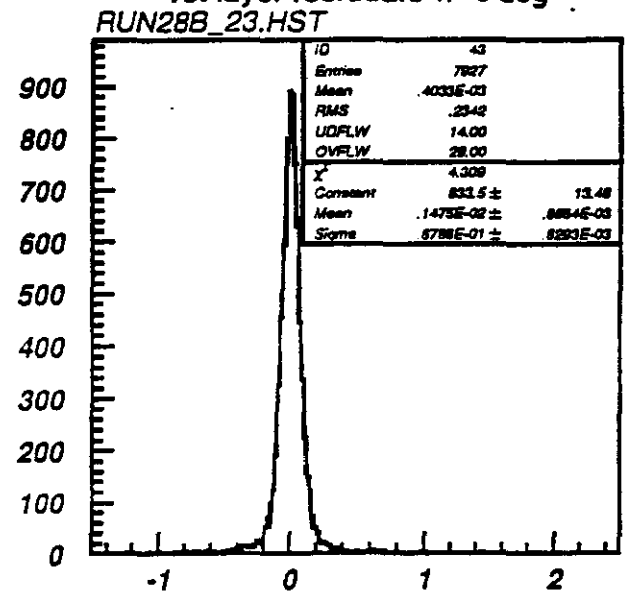

3rd layer residuals +/- 6 deg

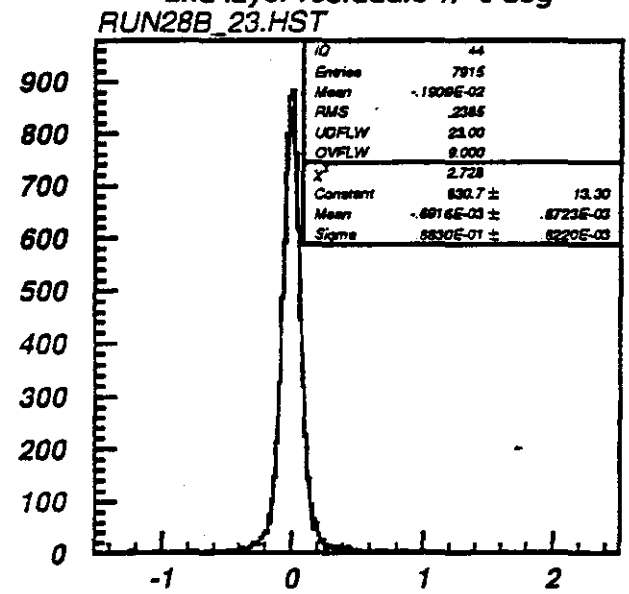

4th layer residuals +/- 6 deg

Fig 22

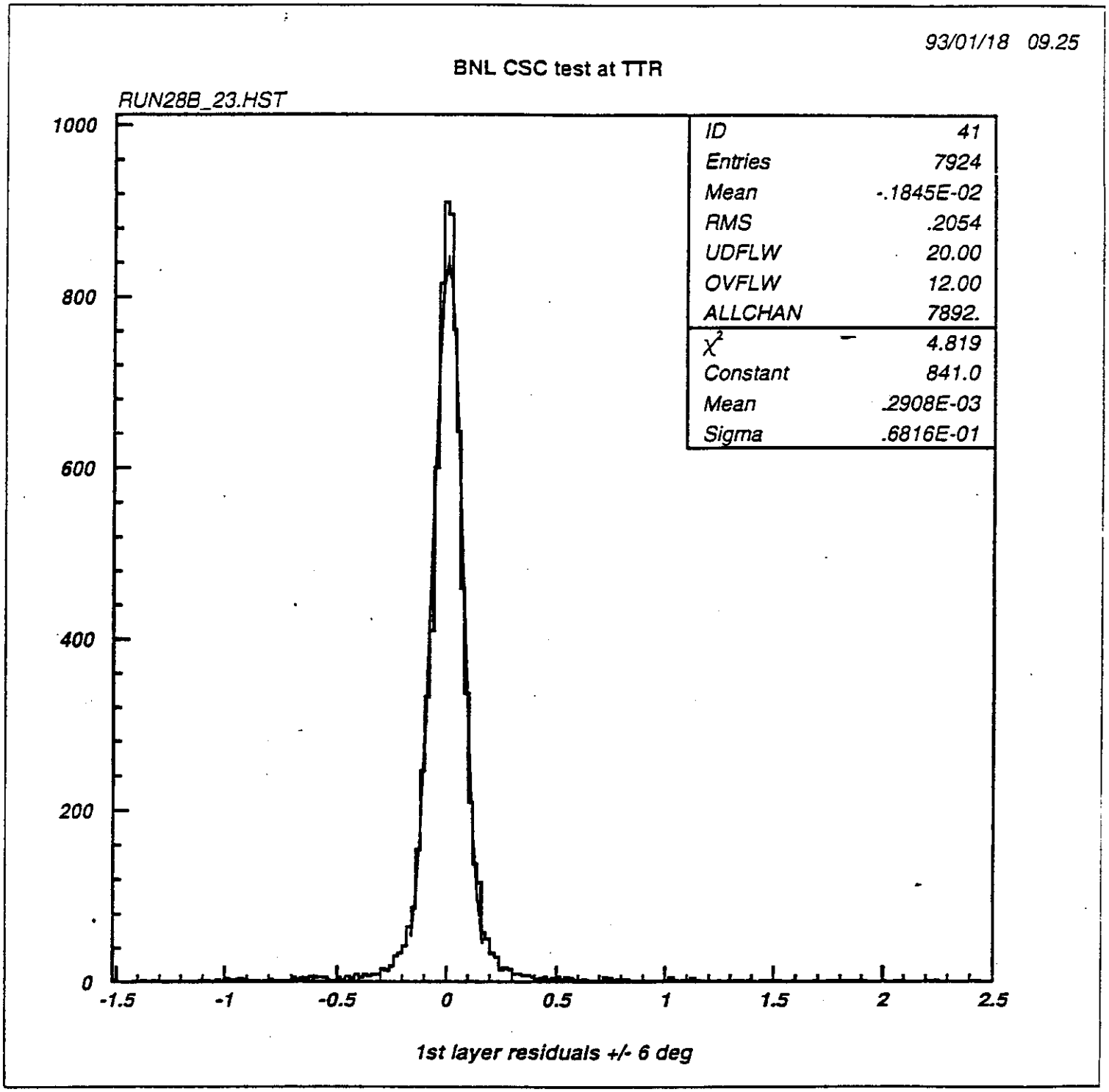
93/01/18 09.25
BNL CSC test at TTR
RUN28B_23.HST
ID 41
Entries 7924
Mean -.1845E-02
RMS .2054
UDFLW 20.00
OVFLW 12.00
ALLCHAN 7892.
χ² 4.819
Constant 841.0
Mean .2908E-03
Sigma .6816E-01
1000
800
600
400
200
0
-1.5
-1
-0.5
0
0.5
1
1.5
2
2.5
1st layer residuals +/- 6 deg

Fig 23

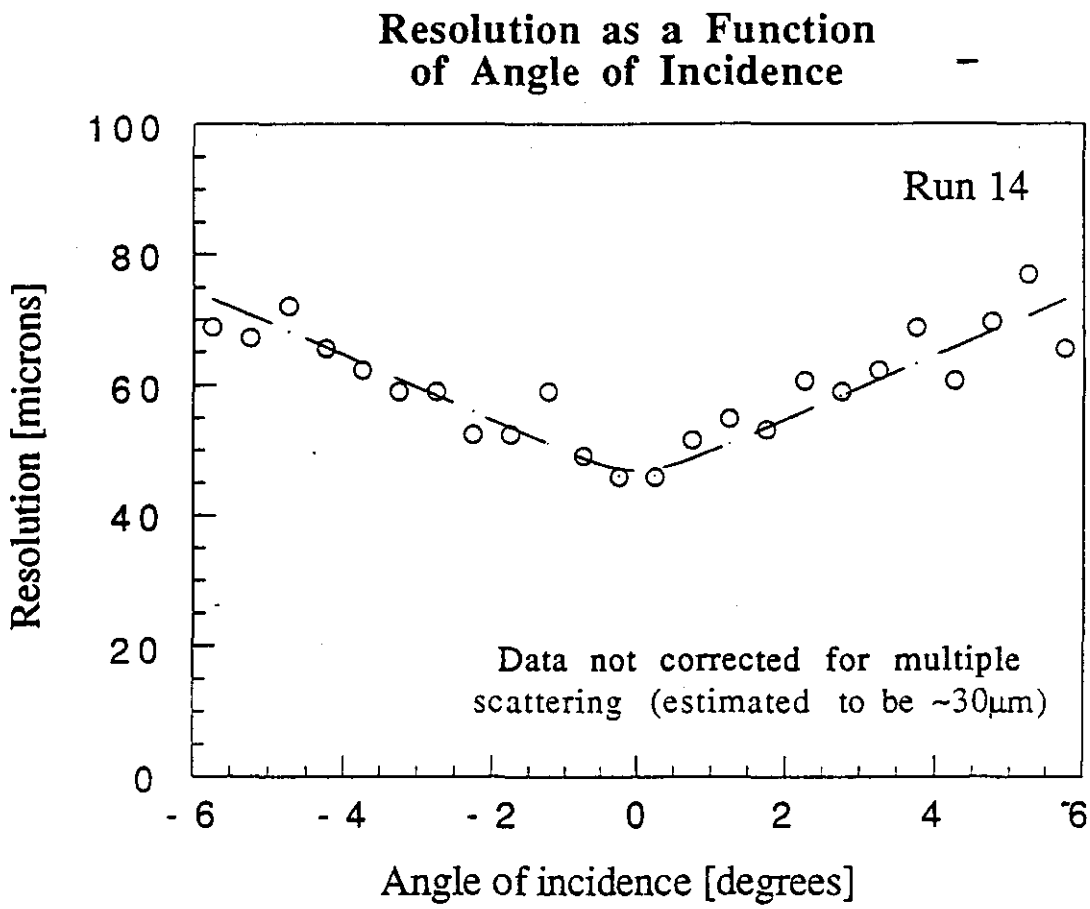
Resolution as a Function
of Angle of Incidence
Run 14
Data not corrected for multiple
scattering (estimated to be ~30μm)
Resolution [microns]
100
80
60
40
20
0
- 6
- 4
- 2
0
2
4
6
Angle of incidence [degrees]

Fig 24

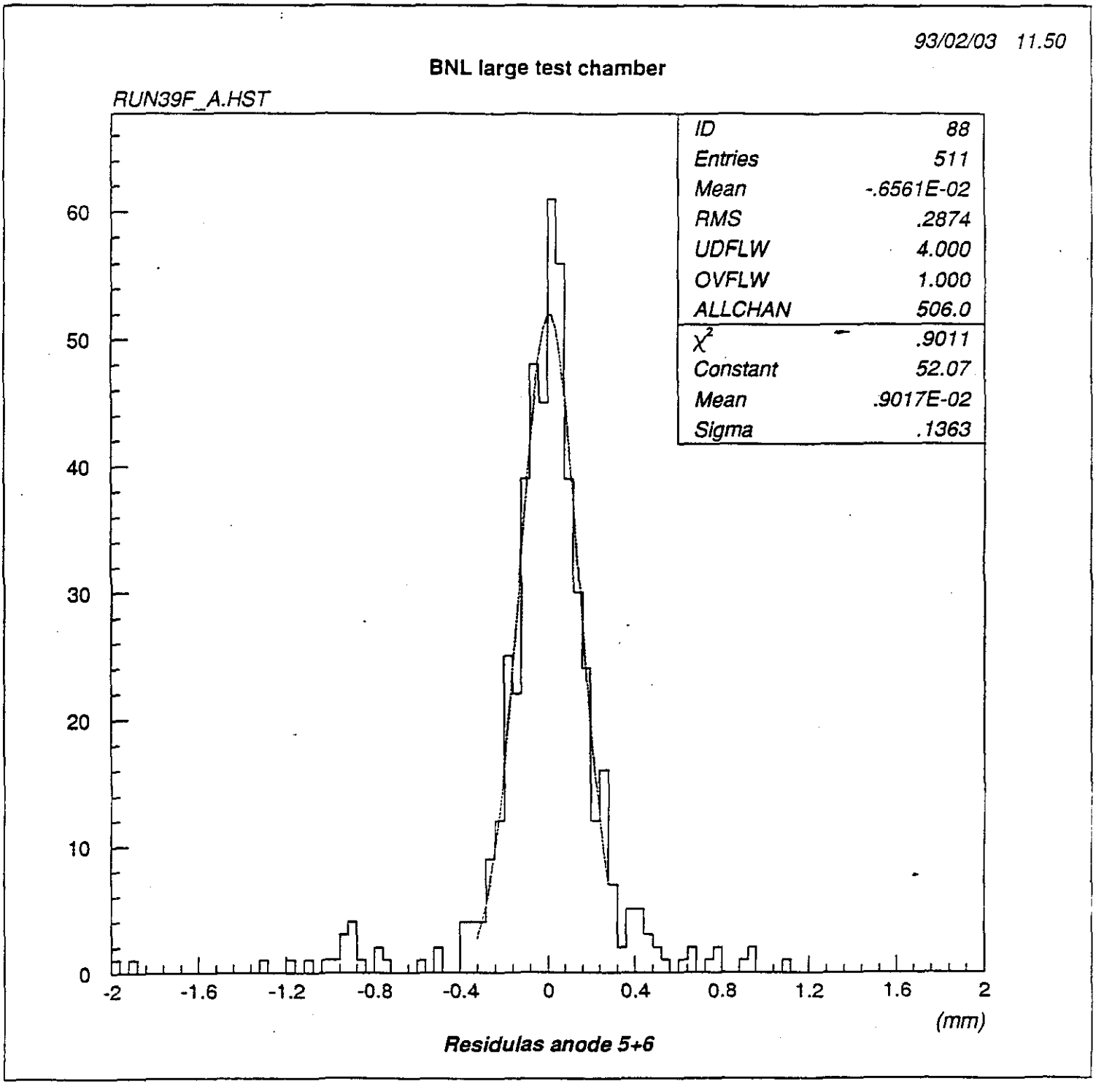
93/02/03 11.50
BNL large test chamber
RUN39F_A.HST
ID 88
Entries 511
Mean -.6561E-02
RMS .2874
UDFLW 4.000
OVFLW 1.000
ALLCHAN 506.0
χ² .9011
Constant 52.07
Mean .9017E-02
Sigma .1363
60
50
40
30
20
10
0
-2
-1.6
-1.2
-0.8
-0.4
0
0.4
0.8
1.2
1.6
2
(mm)
Residulas anode 5+6

Fig 27

Dubna CSC resolution

Resolution

93/01/16 15.24

run 1127

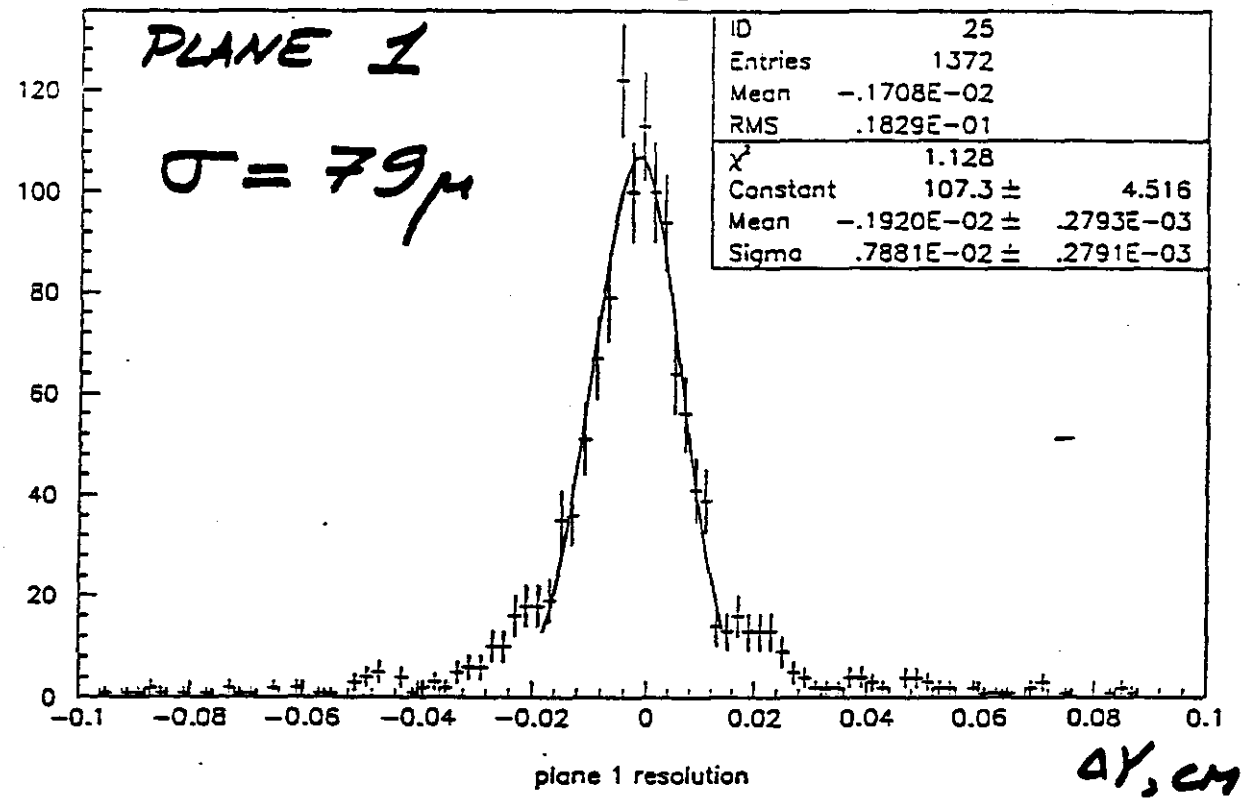

plane 1 resolution

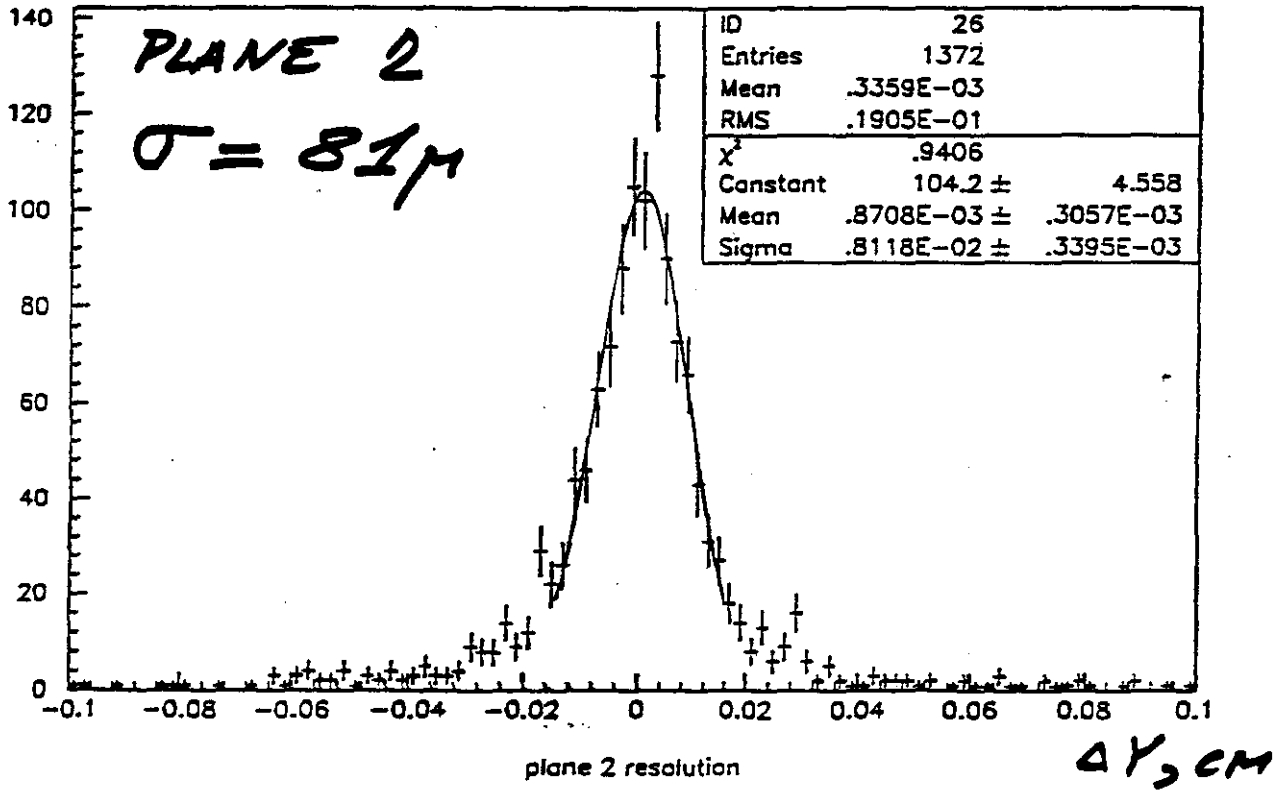

plane 2 resolution

4 inner channels in the same preamp chip

Fig 25

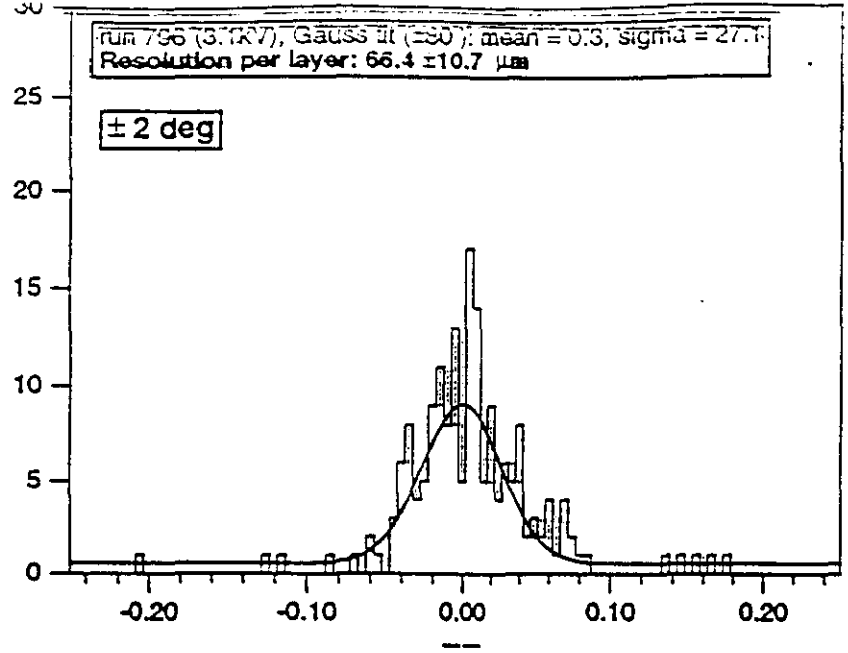
Resolution per layer: 66.4 ±10.7 μm
± 2 deg
0
5
10
15
20
25
30
-0.20
-0.10
0.00
0.10
0.20

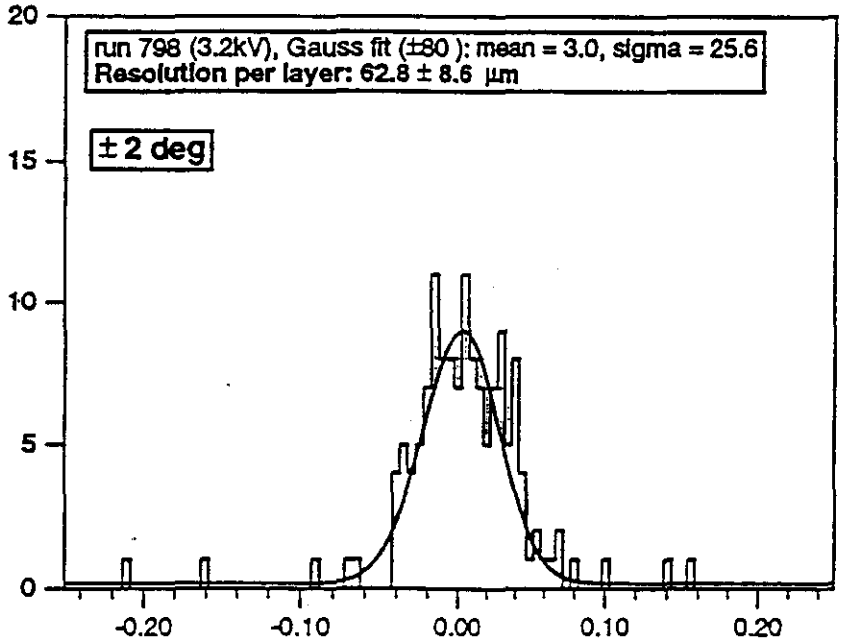
run 798 (3.2kV), Gauss fit (±80): mean = 3.0, sigma = 25.6
Resolution per layer: 62.8 ± 8.6 μm
± 2 deg
0
5
10
15
20
-0.20
-0.10
0.00
0.10
0.20

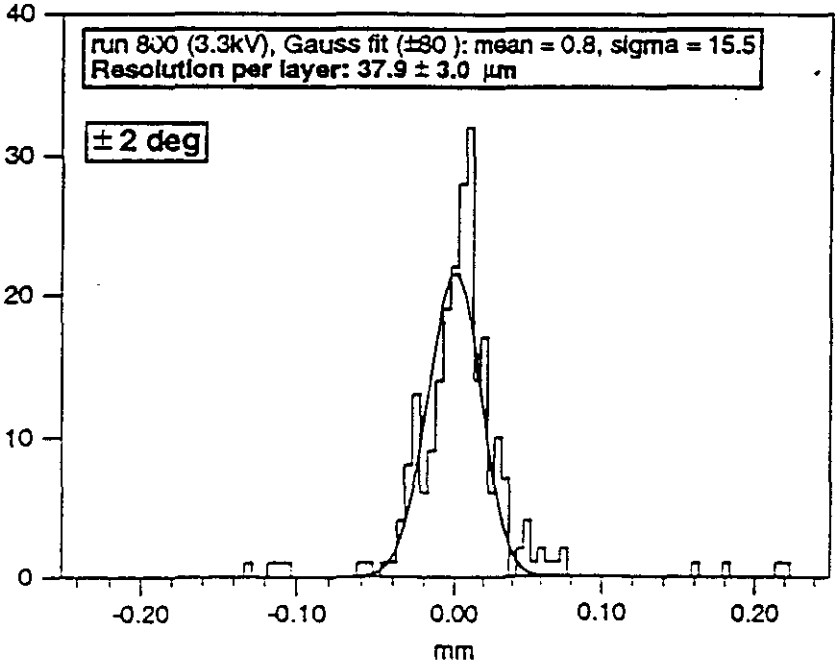
run 800 (3.3kV), Gauss fit (±80): mean = 0.8, sigma = 15.5
Resolution per layer: 37.9 ± 3.0 μm
± 2 deg
0
10
20
30
40
-0.20
-0.10
0.00
0.10
0.20
mm

III a

Efficiency

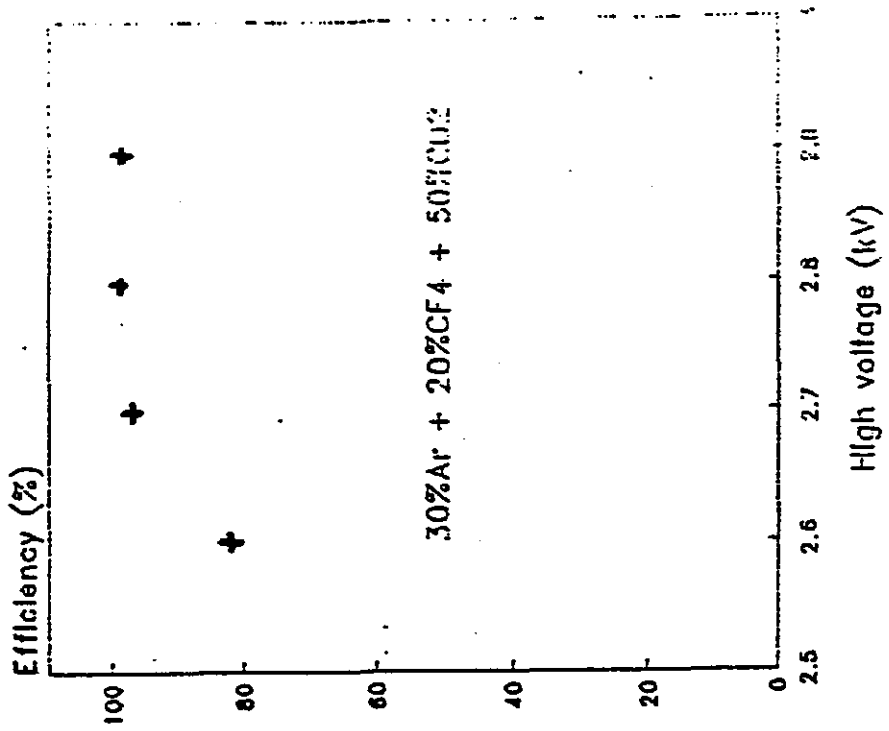

99.8% efficiency

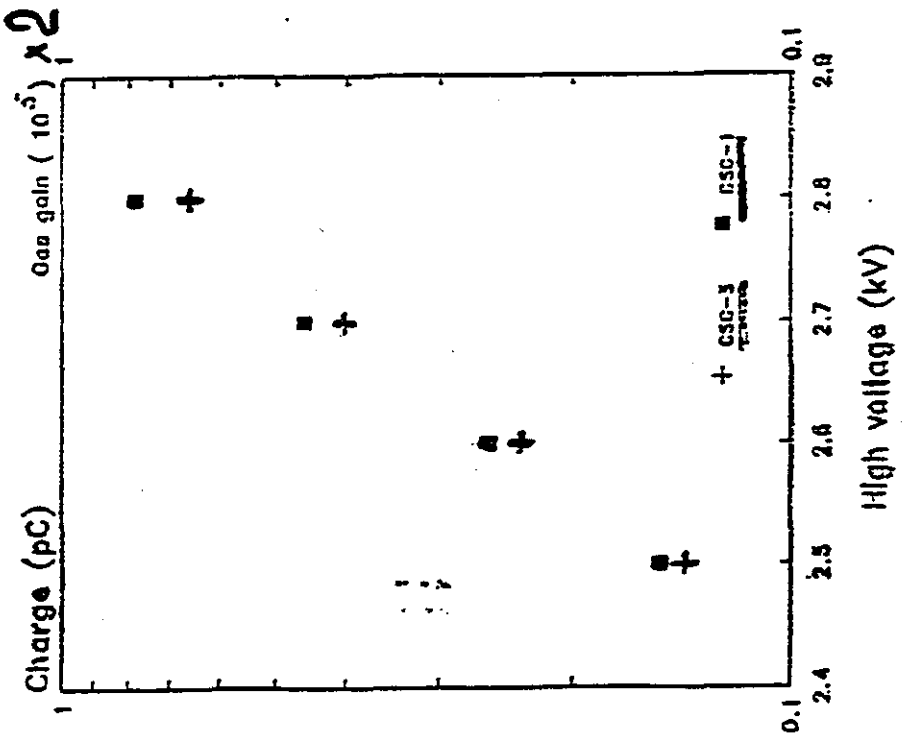

20% difference in gain

Fig. 28

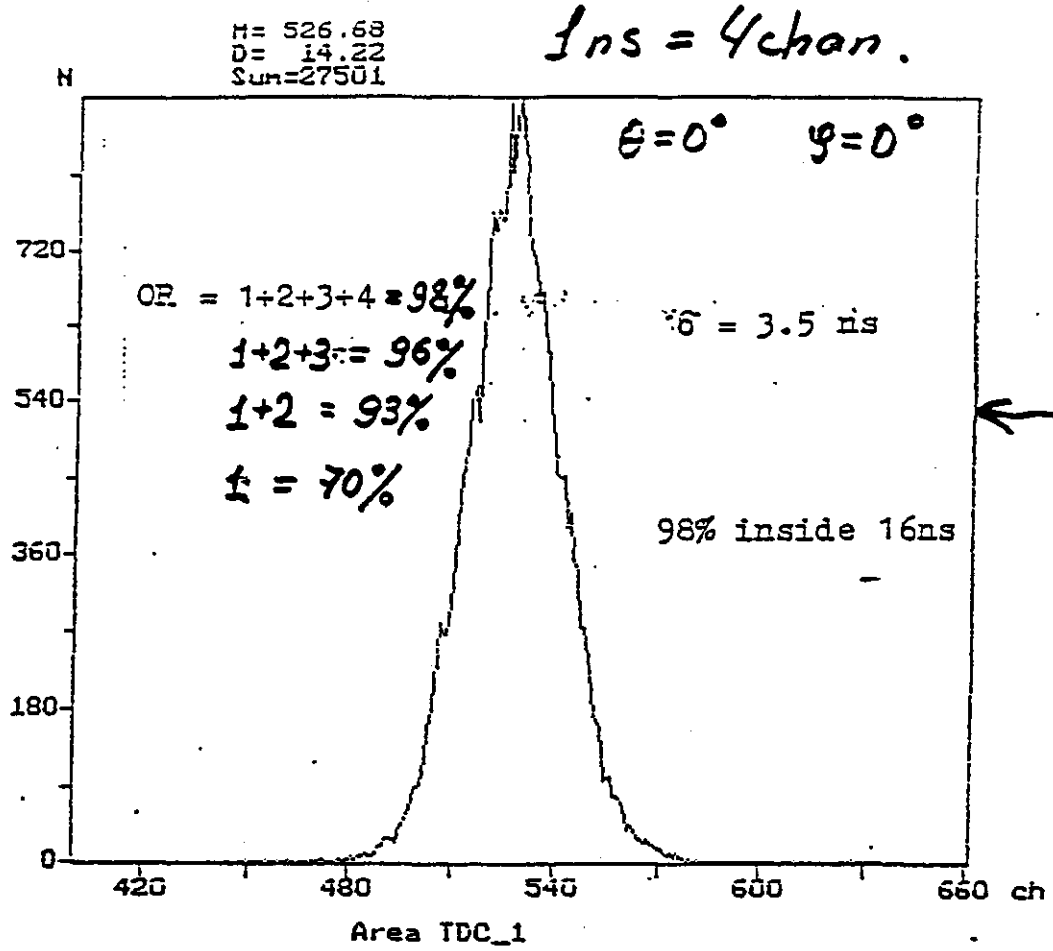

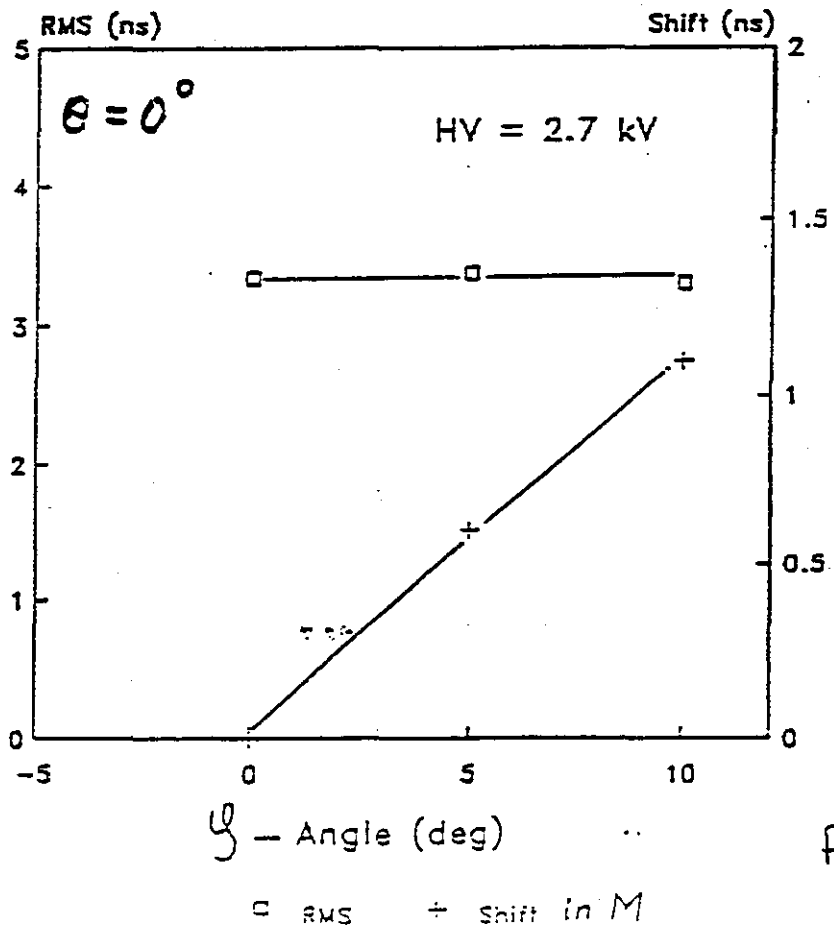

HV = 2.7 kV
σ = 3.5 ns

Fig 29